On the Possibility of Uphill Intramolecular Electron Transfer in Multicopper Oxidases: Electrochemical and Quantum Chemical Study of Bilirubin Oxidase

Shleev, Sergey; Andoralov, Viktor; Falk, Magnus; Reimann, Curt; Ruzgas, Tautgirdas; Srnec, Martin; Ryde, Ulf; Rulisek, Lubomir

Published in:
Electroanalysis

DOI:
10.1002/elan.201200188

2012

On the possibility of uphill intramolecular electron transfer in multicopper oxidases: Electrochemical and quantum chemical study of bilirubin oxidase

Sergey Shleev, [‡,†,*] Viktor Andoralov, [†,#] Magnus Falk,[†] Curt T. Reimann,[‖] Tautgirdas Ruzgas,[†] Martin Srnec,[§] Ulf Ryde,[&] and Lubomír Rulíšek [§,*]

[‡] *The Laboratory of Chemical Enzymology, A.N. Bach Institute of Biochemistry RAS, 119071 Moscow, Russia*
[†] *The Department of Biomedical Sciences, Malmö University, 205 06 Malmö, Sweden*
[#] *The laboratory of Electrocatalysis and Fuel Cells, A.N. Frumkin Institute of Physical Chemistry and Electrochemistry RAS, 119071 Moscow, Russia*
[‖] *Department of Pure and Applied Biochemistry,* [&] *Department of Theoretical Chemistry, Lund University, 22100 Lund, Sweden*
[§] *Institute of Organic Chemistry and Biochemistry, Gilead Sciences Research Center at IOCB, Academy of Sciences of the Czech Republic, 166 10 Praha 6, Czech Republic*

Keywords: Bilirubin oxidase; T1 copper site; T2/T3 copper cluster; Intramolecular electron transfer; Rate-limiting catalytic step, Reorganization energy, QM/MM calculations

*** Corresponding authors.**

A.N. Bach Institute of Biochemistry RAS, 119071 Moscow, Russia
Fax: +7 495 954 2732.
E-mail address: shleev@inbi.ras.ru (S. Shleev).

Institute of Organic Chemistry and Biochemistry, Gilead Sciences Research Center at IOCB, AS CR, 166 10 Praha 6, Czech Republic.
E-mail address: lubos@uochb.cas.cz (L. Rulíšek).

Abstract

The catalytic cycle of multicopper oxidases (MCOs) involves intramolecular electron transfer (IET) from the Cu-T1 copper ion, which is the primary site of the one-electron oxidations of the substrate, to the trinuclear copper cluster (TNC), which is the site of the four-electron reduction of dioxygen to water. In this study we report a detailed characterization of the kinetic and electrochemical properties of bilirubin oxidase (BOx) – a member of MCO family. The experimental results strongly indicate that under certain conditions, *e.g.* in alkaline solutions, the IET can be the rate-limiting step in the BOx catalytic cycle. The data also suggest that one of the catalytically relevant intermediates (most likely characterized by an intermediate oxidation state of the TNC) formed during the catalytic cycle of BOx has a redox potential close to 0.4 V, indicating an uphill IET process from the T1 copper site (0.7 V) to the Cu-T23. These suggestions are supported by calculations of the IET rate, based on the experimentally observed Gibbs free energy change and theoretical estimates of reorganization energy obtained by combined quantum and molecular mechanical (QM/MM) calculations.

1. Introduction

Multicopper oxidases (MCOs), such as bilirubin oxidase (BOx), laccase (Lc), ascorbate oxidase (AOx), and ceruloplasmin (Cp), catalyze the oxidation of different organic and inorganic compounds with concomitant reduction of O_2 to H_2O (Fig. 1, left part) [1]. These enzymes contain four copper ions, which are classified into three types denoted Cu-T1, Cu-T2, and a Cu-T3 pair [2]. The latter two sites form a trinuclear copper cluster (TNC), alternatively termed the Cu-T23 site (Fig. 1).

The mechanism of the MCO function includes three major steps (marked in Fig. 1 as processes 1, 2, and 3), *viz.* (1) electron transfer (ET) from reduced substrates (homogeneous natural reactions [1-3]) or electrodes (heterogeneous artificial catalysis [3-6]) to a mononuclear Cu-T1 site, (2) intramolecular ET (IET) *via* a highly conserved Cu-T1-Cys–$(His)_2$-$(Cu\text{-}T3)_2$ bifurcated ET pathway across a distance of ~13 Å (Fig. 1, dotted arrows), and (3) O_2 reduction to two H_2O molecules within the TNC [2]. The generally accepted view of the overall mechanism of MCOs assumes that the rate-limiting step in homogeneous catalysis of different MCOs is the oxidation of the substrate by the Cu-T1 site (Fig. 1, left part, process 1), whereas the IET and the O_2 reduction are considered to be fast processes, > 1000 s^{-1} [7-10]. On the other hand, the presence of a slow IET (Fig. 1, process 2) for certain forms of MCOs, *e.g.*, for inhibited enzymes [11, 12] and for their resting forms [1, 9, 13, 14], has been also postulated. This observation was further corroborated by detailed bioelectrochemical studies of adsorbed high-redox-potential Lc and Box. It was concluded that under certain conditions, the rate-determining process during bioelectrocatalytic reduction of O_2 can be the IET between the Cu-T1 site and the TNC [15, 16]. Recently, it has also been suggested that the IET might be the limiting step during both artificial (heterogeneous bioelectrocatalysis) and natural (homogeneous catalysis) functions of the MCO [5, 17].

In order to understand the mechanism of the IET in MCOs, information about the redox potentials of the Cu-T1 site (E_{T1}) and the Cu-T23 site (E_{T23}) is obviously needed. The Cu-T1 site can be readily understood since only one E_{T1} value exist as a consequence of the fact the Cu-T1 site contains only one copper ion, which does not coordinate O_2 and therefore is not associated with the formation of different enzyme intermediates. The experimentally observed E_{T1} of different MCOs varies from 0.34 V up to 0.8 V (all potentials in this article refer to the normal hydrogen electrode) [6] and the MCOs are classified according to these values as low-, middle-, and high-redox-potential enzymes. For example, E_{T1} values of high-redox-potential MCOs, *e.g.* fungal Lcs and BOxs, were measured by traditional potentiometric methods and found to be in the range of 0.65–0.78 V [6, 18, 19].

In contrast, the E_{T23} values of MCOs are difficult to measure directly by traditional potentiometric methods, because redox titrations can only be performed in the absence of the O_2 (which is the substrate of the enzyme) and therefore, these methods cannot yield the E_{T23} of various short-lived intermediates formed during the catalytic cycle. Moreover, taking into account the great number of redox transitions

of the Cu sites accompanying four IET steps during one catalytic turnover of MCOs [1, 9, 20-22], several redox potentials of the Cu-T23 cluster (E_{T23}) are expected. These unknown E_{T23} values are *a priori* considered to be very high [16], because some intermediates of MCOs are expected to be highly reactive and strongly oxidizing [9]. However, previous electrochemical investigations allowed us to suggest that one of the intermediates of the Cu-T23 cluster of high-redox-potential MCO has a quite low E_{T23}, close to 0.4 V [5, 23]. Similar (~0.4 V) midpoint potentials (E_{mp}) are also observed for high-redox-potential Lc under both anaerobic and aerobic conditions [5, 6, 19, 23-29]. Considering that the redox potential of Cu-T1 of high-potential MCOs (E_{T1}) is 0.65–0.78 V, this implies that at least one of the IET sub-processes occurring during the reduction of the Cu-T23 site (process 2 in Fig. 1; which requires four electrons in total [9, 20]) is an endoergic (uphill) process, which might limit the overall rate of the catalytic activity of BOx under certain conditions. This is supported by the recent observation of a slow IET process during BOx-catalyzed electroreduction of O_2 in alkaline solutions [16].

BOx (bilirubin:oxygen oxidoreductase, EC 1.3.3.5) is a MCO that catalyzes the oxidation of bilirubin (BR) to biliverdin (BV) (Fig. 1, left part). BOx has been widely used for a long time in clinical analysis [30, 31] and biofuel cells [32-36], but the crystal structure was published only recently [37, 38]. It is a highly similar to structures of other MCO and BOx contains a full complement of four copper ions per monomer, located in domains 1 and 3 [37, 38]. In recent years, BOx from two sources, *Myrothecium verrucaria* and *Trachyderma tsunodae* BOx (*Mv*BOx and *Tt*BOx) have also been characterized electrochemically [4-6, 16, 19, 39, 40] and the redox potentials of the Cu-T1 sites (E_{T1}) of both BOx were determined to be approximately 0.7 V using mediated and mediatorless cyclic voltammetry (CV) and redox titrations [5, 18, 19]. Therefore, *Mv*BOx and *Tt*BOx can be classified as high-redox-potential MCOs, which is an important property for biofuel cell applications.

The aim of the present work is to obtain a deeper insight into the function of these enzymes. To this aim, we performed detailed kinetic and voltammetric studies of highly purified *Tt*BOx and *Mv*BOx in a very broad pH range. We relate these new data to results of our previous work with BOx [5, 6, 19, 39], as well as to other available spectral, kinetic, and electrochemical data of different MCOs [2-4, 9, 12, 16, 18, 27, 29, 40-50]. These data are further complemented by combined quantum mechanical and molecular mechanics (QM/MM) calculations of reorganization energies (λ) accompanying the studied ET processes. Owing to the complicated electronic structure of the TNC, as well as the complex surrounding of the Cu-T23, we consider QM/MM approach as the optimal computational strategy. Recently, QM/MM calculations were used to elucidate the reaction catalytic cycle of MCOs [20, 51] provide a structural interpretation of the spectroscopic data [52], and directly correlate the structure of MCO intermediates with the experimental EXAFS data [53] using an original QM/MM-EXAFS coupling scheme. Moreover, QM/MM molecular dynamics simulations have been used to calculate the E_{T1} and λ values of the Cu-T1 site in different MCO [54]. These studies clearly demonstrated that

theoretical calculations (particularly QM/MM), when correlated with experimental data, provide an invaluable source of information for understanding the details of enzymatic action in systems as much complicated as MCOs; all these computational achievements have been summarized in the recent comprehensive review [55].

2. Experimental

2.1. Reagents

Na_2HPO_4, NaOH, KH_2PO_4, H_3PO_4, CH_3COOH, KCl, NaCl, NaF, $K_4[Fe(CN)_6]$, H_3BO_3, and $NaClO_4$ were obtained from Merck (Darmstadt, Germany). $K_4[Mo(CN)_8]$, carbon nanopowder (CNP), and citric acid were from Sigma-Aldrich (St. Louis, MO, USA). All chemicals were of analytical grade.

Buffers were prepared with water (18 MΩ·cm) purified with a PURELAB UHQ II system from ELGA Labwater (High Wycombe, UK). Different oxygen concentrations were established using nitrogen, air, and oxygen from AGA Gas AB (Sundbyberg, Sweden). Nitrogen (N_2) was additionally purified using Gas Clean Filters from Varian BV (Middelburg, The Netherlands).

2.2. Enzymes

BOx from *T. tsunodae* was kindly provided by Dr. Nicolas Mano (Centre de Recherche Paul Pascal, France). According to the provider, the enzyme was homogeneous as judged from SDS-PAGE and mass spectrometry. BOx from *M. verrucaria* (Amano 3 preparation) was obtained from Amano Enzyme Inc. (Nagoya, Japan) and was additionally purified and biochemically characterized by Dr. Olga Morozova (A.N. Bach Institute of Biochemistry, Moscow, Russia). All preparations were stored at –20°C and were used without further purification. The concentration of the enzymes in the stock solutions was determined by the method of Ehresmann [56] and compared with a direct method based on the optical absorbance at 610 nm, which is characteristic of the type-1 cupric ion of BOx, using a molar absorption coefficient (ε) of 3870 $M^{-1}cm^{-1}$ [43].

2.3. Kinetic studies

The kinetic investigation of *Mv*BOx was performed by estimation of the initial rates of O_2 consumption by using an Oxygraph Clark oxygen electrode from Hansatech Ltd. (Norfolk, England) at 25°C with constant stirring. Appropriate concentrations of transition metal cyanide complexes ($K_4[Fe(CN)_6]$ and $K_4[Mo(CN)_8]$) and ABTS dissolved in air-saturated 0.05 M universal buffer with different pH values (a mixture of 50 mM of phosphoric acid, boric acid, and acetic acid adjusted to the desired pH using NaOH) and appropriate concentration of the enzymes (~20 *p*M) were used in order to ensure a measurable linear rate for the first 60 sec of enzymatic reactions initiated by the addition of

*Mv*BOx. Control experiments were also performed in which no enzyme was used and oxygen reduction rates in these cases were negligible.

The apparent Michaelis constants (K_M) of BOx towards O_2 were determined in 0.1 M phosphate buffer pH 7.0 using $K_4[Fe(CN)_6]$ as the electron donor at a fixed concentration of 5 mM, *i.e.*, significantly higher than the K_M for this substrate. Different concentrations of O_2 were established by bubbling N_2 through an oxygraph cell for certain periods of time.

All kinetic parameters were calculated using the Michaelis–Menten equation in the Microcal Origin program (version 5.0).

2.4. Electrochemical measurements

Electrochemical measurements were performed using a three-electrode EC Epsilon potentiostat/galvanostat (Bioanalytical Systems (BAS), West Lafayette, IN). The reference electrode was a $Hg|Hg_2Cl_2|KCl_{sat}$ electrode K401 (SCE; 0.242 V) from Radiometer (Copenhagen, Denmark), and the counter electrode was a platinum wire mesh. Two types of working electrodes were used, *viz.*, a spectrographic graphite electrode (SPGE), and a glassy carbon electrode (GCE) from BAS with an ultrathin layer (*ca.* 1 μm) of CNP.

SPGE for use as a working electrode was prepared by polishing the end of a rod of spectrographic graphite (Ringsdorff Werke GmbH, Bonn, Germany, type RW001, 3.05 mm diameter, 13% porosity) with wet fine Tufback Durite emery paper, P1200 (Allar Co., Sterling Heights, MI, USA) and inserting the rod into a Teflon holder. The SPGE was then rinsed thoroughly with UQH H_2O and allowed to dry. The detailed characterization of the spectrographic graphite used in our studies is given in Ref. [57].

GCE modified with CNP (CPGCE) was prepared following a procedure described in Refs. [58, 59]. Briefly, the GCE was cleaned by polishing on Microcloth (Buehler) in an aqueous alumina FF slurry (0.1 μm, Stuers, Denmark). The electrode was treated in an ultrasound bath for 10 min, rinsed with UHQ water, and allowed to dry. An aliquot of an aqueous suspension of CNP (3 mg ml^{-1}) was deposited on the electrode surface and dried at room temperature. The aliquot volume was chosen to give final surface mass densities of CNP in the of 20–400 μg cm^{-2}. According to the provider (Sigma-Aldrich), CNP has a particle size < 500 nm, average pore diameter of about 6.4 nm, and specific surface area of *ca.* 200 m^2 g^{-1}.

All working electrodes were biomodified by a simple adsorption of the enzyme on the electrode surface. A drop of solution containing enzyme (10 mg/ml; 5 μl) was evenly deposited on the top of electrodes, adsorbtion was allowed to occur, and after 10 min the electrode was carefully rinsed with H_2O. It should be emphasized that the electrodes did not dry out at any time during bio-modification. However, additional studies have shown almost no difference in electrode performances in the event that an electrode surface dries during immobilization prior to rinsing.

All potentials in this work are given *vs.* NHE. The current densities were calculated using a geometric area of both electrodes equal to 0.07 cm^2. All measurements were performed at 25°C.

2.5. Computational details

All QM/MM calculations were carried out with the COMQUM program [60, 61] with Turbomole 5.7 [62] used for the quantum mechanical (QM) part and AMBER 8 [63] with the Cornell force field [64] for the molecular mechanics (MM) part. The QM calculations were performed at the density functional theory (DFT) level. Geometry optimizations were carried out at the Perdew–Burke–Ernzerhof (PBE) level [65]. The DFT/PBE calculations were expedited by expanding the Coulomb integrals in an auxiliary basis set, the resolution-of-identity (RI-J) approximation [66]. The def2-SVP basis set was employed for all atoms [67]. Single-point energies were then calculated using the B3LYP method [68], as implemented in Turbomole 5.7, and the def2-TZVP basis set [67].

In the QM/MM approach, the protein and solvent are split into three systems. The QM region, system 1, contains the atoms for which the most detailed calculations are desired and is relaxed by QM/MM forces and in our case it contained 80 atoms. All amino-acid residues within 6 Å of any atom in system 1 comprise system 2, which is relaxed by a full MM minimization in each step of the QM/MM geometry optimization of system 1 (1050 atoms). Finally, system 3 consists of the remaining parts of the protein and surrounding solvent molecules and is kept fixed at the original (crystallographic) coordinates.

As in our previous work [20], all QM/MM calculations were based on the 1.4 Å structure of CueO (PDB code 1KV7; Fig. 1) [69]. This structure was selected because it had the best resolution among the published MCO structures at the start of this computational investigation, when the BOx crystal structure was still unknown. It has 21% homology with *Mv*BOx, which is slightly less than that of another member of the MCO family, CotA (31%). However, we preferred to be consistent with our previous work [20, 52, 53] and use the better-resolution structure. The system was solvated in a sphere of water molecules with a radius of 38 Å. As mentioned in our previous work [20], the missing loop in the crystal structure (residues 380-402) was omitted in the calculations (the empty space was filled by water molecules). We assumed the normal protonation state at pH 7 for all amino acids, except for the copper-bound (T1) Cys residue, which was considered to be deprotonated. Further details concerning the protonation of the histidine residues, the structure setup, and the QM/MM procedure can be found in Ref. [20]. Eight histidine residues on the surface of the protein were considered to be protonated on both nitrogen atoms (His145, 224, 314, 405, 406, 465, 488, and 494 in the 1KV7 structure), whereas all ten metal-binding His residues were of course protonated only on the nitrogen atom not coordinating to Cu. All calculations on the Cu-T23 cluster were carried out for the high-spin states (ferromagnetically-

coupled copper ions). It has been shown that the splitting between low- and high-spin states is in most cases ~0.05 eV [20], which is below the estimated error of the calculated λ.

The λ values associated with a system undergoing a transition from an initial state to a final state is in general defined as

$$\lambda = E(\text{final state//initial state}) - E(\text{final state//final state}) \quad (1)$$

where E(A//B) denotes the total QM/MM energy of state A at the geometry optimized for state B. When A = B, we use the notation E(A/opt) instead of E(A//A). Consider the transfer of an electron from the Cu-T1 site to the Cu-T23 cluster (Fig. 1), *i.e.* the formal reaction

$$T1^{(+)} + T23^{(6+)} \rightarrow T1^{(2+)} + T23^{(5+)} \quad (2)$$

Here, we assume that we study the oxidized or native intermediate (NI) state of the Cu-T23 cluster. We arrive at the following expression for λ:

$$\lambda = E(T1^{(2+)}\ldots T23^{(5+)}//T1^{(+)}\ldots T23^{(6+)}) - E(T1^{(2+)}\ldots T23^{(5+)}/\text{opt}) \quad (3)$$

Unfortunately, it is impractical to evaluate λ directly in QM/MM calculations. This would involve the use of one quantum system comprising both Cu-T1 site and Cu-T23 cluster and the necessity to calculate two distinct electronic states (of which one would be an electronically excited state) corresponding to the initial and final (after ET) states. We made several attempts to carry out this task, but found it prohibitively difficult. Therefore, we use the following plausible approximation:

$$\lambda \approx \lambda_1 + \lambda_2 \quad (4)$$

where λ_1 and λ_2 are the reorganization energies of the Cu-T1 site and Cu-T23 cluster, respectively.

$$\lambda_1 = E(T1^{(2+)}//T1^{(+)}) - E(T1^{(2+)}/\text{opt}) \quad (5)$$

$$\lambda_2 = E(T23^{(5+)}//T23^{(6+)}) - E(T23^{(5+)}/\text{opt}) \quad (6)$$

When calculating *e.g.* λ_1, the status of Cu-T23 cluster may be important even though it does not appear explicitly in the equation. In the calculation of λ_1, the QM region (system 1) would comprise the

Cu-T1 site, while the Cu-T23 cluster would lie in the MM region (system 2). However, as a best approximation, the geometry and MM parameters (point charges) for the Cu-T23 cluster were extracted from the situation where Cu-T23 comprised the QM system, *i.e.* from the previous calculation of λ_2, instead of being taken from the Amber libraries. This results in an iterative approach that improves the accuracy and stability of the calculated reorganization energies. Indeed, we iterated the calculations of λ_1 and λ_2 at least twice: optimizing the A state and then changing it to the B state, optimizing again to obtain the reorganization energy, changing back to A, and so on (where A and B stand for the oxidized or reduced form of the Cu-T23 cluster or the Cu-T1 site).

With the above points in mind, the amino-acid residues comprising the QM region (system 1) in various calculations on CueO can be specified. Two sets of QM/MM calculations were performed: the first with the Cu-T23 cluster and the first-shell coordinating residues as the QM system (and the Cu-T1 site in the MM system) and the second with T1 and its coordinating residues in the QM system (and the Cu-T23 cluster in the MM system, but adopting the optimized QM/MM geometry and point charges for Cu-T23). Therefore, the QM regions in the QM/MM calculations consisted of the following residues: Q1 = the Cu-T1 copper ion, two His residues, one deprotonated Cys residue, and one Met residue. Q2 = the three Cu-T23 copper ions, eight His residues, two water molecules, and the T23-bound O_2-derived species in the NI. The two QM systems are depicted in Figure 1.

Finally, we attempted to estimate the error in the calculated λ values. Assuming that the QM/MM procedure can, in principle, yield values of satisfactory accuracy, there are three sources of error: (1) the difference in the energy splitting between the low- and high-spin states of the copper atoms; (2) reorganization of the solvent, including entropic effects; and (3) the accuracy of the method and basis sets used. While we consider the first error as fairly small (as discussed above), we must admit that we may only assume that the reorganization of the solvent can be neglected. The argument we put forward is that the ET pathway between the Cu-T1 site and Cu-T23 cluster is buried in the interior of the protein and the ET, which does not change the total charge of the protein, should not involve any major reorientation of solvent molecules. A recent methodological study [70] of reorganization energies for a MCO shows that the solvent contribution to λ in MCOs is expected to be ~0.35 eV and that the protein contribution (~0.6 eV) is dominated by residues close to the copper sites.

To assess the last error, that is, the accuracy of the method used for the description of the QM core, we carried out the QM/MM calculations using the def2-TZVP basis set and two functionals: PBE and B3LYP. From these calculations (or the differences in the obtained energies), we deduce that the errors of the QM method can be estimated as 0.05–0.1 eV.

3. Results and Discussion

3.1. Determination of basic kinetic parameters in homogeneous reactions

First, we determined the k_{cat} values of *Mv*BOx for homogeneous enzymatic oxidation of three substrates with different redox potentials (E_S), at six different pH values. The results are presented in Table 1. The k_{cat} values of *Mv*BOx were correlated with the difference in the thermodynamic driving force between the substrates and the T1 copper ($\Delta G_{S\rightarrow T1} = -nF\Delta E_{T1\text{-}S}$), *i.e.* with the redox potential difference ($\Delta E_{T1\text{-}S} = E_{T1} - E_S$) between the electron donor (substrate, E_S) and the first electron acceptor (the Cu-T1 site, E_{T1}). Well-pronounced correlation between the maximal turnover rates of the enzyme towards studied substrates and $\Delta G_{S\rightarrow T1}$ was obtained (k_{cat} for the three substrates follow the trend $K_4[Fe(CN)_6]$ > ABTS > $K_4[Mo(CN)_8]$ for all pH values, except pH = 3.3, in accordance with the same trend for $\Delta E_{T1\text{-}S}$, *cf.* the results in Table 1). Similar dependences have previously been observed for different MCOs including BOx for various sets of substrates [50, 71, 72].

Second, the K_M values towards $K_4[Fe(CN)_6]$, 2,2'-azino-bis(3-ethylbenzothiazoline-6-sulphonic acid (ABTS), and $K_4[Mo(CN)_8]$ were found to be 0.1, 0.08, and 0.15 mM, respectively. Our results are in good agreement with available K_M values of *Mv*BOx towards $K_4[Fe(CN)_6]$ and ABTS reported to be 0.113 mM and 0.076 mM, respectively [72, 73]. The K_M of *Mv*BOx towards O_2, the second natural substrate (electron acceptor) in the catalytic cycle of all MCOs, measured in homogeneous neutral solution (pH 7.0), was found to be ~0.2 mM. This is in good agreement with previously reported K_M values of MCO measured in homogeneous biocatalytic systems (0.1–0.4 mM) [11, 15, 74, 75].

3.2. Electrochemical investigations of BOx under heterogeneous conditions

In order to establish the robustness of our results, as well as to set BOx properties into the broader perspective of the MCO family, detailed electrochemical investigations of BOx for heterogeneous enzymatic reduction of O_2 were performed using various electrochemical techniques, *e.g.* cyclic and linear sweep voltammetries (CVs and LSVs, respectively), amperometry, and potentiometry. In contrast to previous bioelectrochemical studies of BOx [4, 5, 16, 38-40, 76], these investigations have been done over broad potential (0–1.0 V) and pH (2.6–8.2) ranges using two different electrodes and pure preparations of two different enzymes isolated from two different fungi, the ascomycete *Myrothecium verrucaria* and the basidiomycete *Trachyderma tsunodae*.

The electrodes modified with *Tt*BOx or *Mv*BOx were placed in N_2-, air-, and O_2-saturated acidic, neutral, and alkaline solutions and the catalytic current related to bioelectroreduction of O_2 was clearly visible under aerobic conditions for both enzymes in all cases (Figs. 2A and B). This is in excellent agreement with our previously published data [5, 39], as well as with electrochemical results from other groups [4, 16, 40, 76, 77].

Contrary to our previous electrochemical studies of *Tt*BOx using SPGE [5], in which merely high-redox-potential turnover signals on original CVs were clearly observed, while low-redox-potential bioelectrocatalytic processes were visible only on background subtracted voltammograms, detailed investigations of electrochemical signals from *Tt*BOx- and *Mv*BOx-modified electrodes under both aerobic and anaerobic conditions, as well as careful comparison of turnover and non-turnover signals from both enzymes were performed in the present work, as described below.

3.2.1. Trachyderma tsunodae BOx

When electrochemical measurements with homogeneous *Tt*BOx were performed in air-saturated buffer at pH 4.0, a steady-state bioelectrocatalytic response was obtained with a half-wave potential of O_2 reduction at about 0.69 V (Fig. 2A, curve 2), coinciding with the proposed E_{T1} value of the enzyme [5, 18]. The shape of the CV (an almost steady-state potential–current curve with a broad, feeble peak at ~0.35 V) and the observed dependence of the biocatalytic current on the stirring represent a strong evidence for mass-transfer limitations.

When increasing the O_2 concentration with O_2-saturated buffers, the current density increased and an additional well-pronounced catalytic wave appeared in the CVs starting at *ca.* 0.45 V (Fig. 2A, curve 3). A similar sigmoidal wave, although much less pronounced and visible only on the background-subtracted CVs, was obtained at pH 7.0, in excellent agreement with our previously reported data [5]. Importantly, both the starting potential and the half-wave potential of O_2 reduction were nearly independent of the O_2 concentration. The bioelectrocatalytic reduction of O_2 started at a potential of about 0.81 V (pH 4) and changed by about 0.02 V/pH-unit, *i.e.* similar to the pH-dependence of E_{T1} of MCOs [78, 79]. Moreover, this potential is 0.12 V higher than E_{T1} of BOx, and only 0.18 V lower than the thermodynamic reduction potential for the O_2/H_2O couple at the same pH (+0.99 V), which is in agreement with previously published results concerning potential differences (0.2 V [39], 0.09 V [5], and 0.14 V [16]) between the onset of O_2 electroreduction on BOx-modified electrodes and the four-electron O_2/H_2O potential at different pH values (4, 7, and 8, respectively) [5, 16, 39]. To ensure that the general character of the obtained results is related to intrinsic properties of BOx rather than to specific features of a particular enzyme preparation, detailed studies of another BOx were also performed as described in the next section.

3.2.2. Myrothecium verrucaria BOx

In general, all data presented above for homogeneous *Tt*BOx preparations were reproduced with the highly purified BOx from *M. verrucaria* adsorbed on SPGE. In addition, K_M of adsorbed *Mv*BOx towards O_2 was measured in a heterogeneous system at different applied potentials (Supporting Information, Part 1 (SI1), Fig. S1). The constants obtained at two potentials applied to the electrode, *i.e.*

at very low and high overpotentials (0.11 mM and 0.27 mM at 0.5 and 0.05 V, respectively), are in good agreement with recently reported K_M values of *Mv*BOx measured using another heterogeneous bioelectrocatalytic system, *viz.* *Mv*BOx-modified pyrolytic graphite 'edge' electrodes [16].

In spite of the fact that SPGE is well-characterized [57] and widely used for MCO studies [39, 79, 80], it is not a very good electrode for fundamental bioelectrochemical investigations of redox proteins. First, SPGE is not an ideally non-polarizable electrode: initial parts of the cathodic and anodic branches of the CV displayed an extended arc-like shape due to the distribution of ohmic losses in the porous layer of the electrode (SI1, Fig. S2). Moreover, under certain conditions, the occurrence of some electrochemical processes on this surface could be seen. By contrast, the CV of CPGCE is symmetric and initial parts of the cathodic and anodic branches of the voltammogram display a clear step (Fig. S2). Second, an enzyme can penetrate into the bulk of SPGE upon surface biomodification, so that a porous biomodified electrode with indefinite thickness is obtained. Finally, a system similar to a gas diffusion electrode, when O_2 from a gas phase penetrates to a bioelectrochemically active layer built on SPGE, might be created. Thus, to improve the quality of the data and work towards achieving better insight into the function of BOx, detailed voltammetric studies of highly purified *Mv*BOx were also performed using another electrode, CPGCE, which lacks most of disadvantages described above.

First, *Mv*BOx-modified CPGCEs were placed in N_2-, air-, and O_2-saturated acidic, neutral, and alkaline solutions and the catalytic current related to bioelectroreduction of O_2 was clearly visible under aerobic conditions. For stationary biomodified electrodes, diffusion limitation was registered even under O_2-saturated conditions. This is not surprising because, unlike in experiments on *Tt*BOx-modified SPGE (Fig. 2A, curve 2), O_2 was not bubbled through the buffer during the measurements. However, if the electrode was rotated at high speed, almost no diffusion limitations was observed, as was confirmed in additional studies of the dependence of bioelectroreduction of O_2 on the rotation rate of *Mv*BOx-modified CPGCE (SI1, Fig. S3). Nevertheless, two bioelectrocatalytic waves could be seen for both stationary and rotated biodevices (Fig. 2B). However, when the bioelectrocatalytic process was limited by O_2 diffusion, the second wave was significantly attenuated (Fig. 2B, *cf.* curves 2 and 3), in agreement with the results obtained for *Tt*BOx-modified SPGE described above (*cf.* curves 2 in Fig. 2A and 2B).

To ensure the absence of diffusion limitations inside the porous three-dimensional biostructure based on *Mv*BOx-CNP, investigations concerning the loading of GCE with biomodified CNP were performed. A linear dependence of bioelectrocatalytic current on GCE loading was obtained up to 200 μg cm^{-2} of CNP, starting from 0, indicating the absence of diffusion limitation and porous layer influence, as well as pointing to the biocatalytic nature of the obtained currents (SI1, Fig. S4). Consequently, CPGCE with 200 μg cm^{-2} of CNP loading was used in all further studies.

Second, a redox transformation of BOx under anaerobic conditions was clearly observed on *Mv*BOx-based CPGCE (Fig. 3A), in analogy with published results for *Tt*BOx adsorbed on SPGE (see Fig. 1 in

Ref. [5]). Two redox processes were registered, *viz.* high- and low-redox-potential transformations. The low-redox-potential process was almost reversible (ΔE_p = 0.03 V), whereas the high-redox-potential process was quasi-reversible (ΔE_p = 0.15 V). Calculation of the surface concentration of electroactive *Mv*BOx (Γ) from the charge associated with the waves and the area of the electrodes provided the total coverage of 6.7 pmol per one CPGCE, *i.e.* ~94 pmol cm^{-2} (geometric area), assuming an exchange of four electrons per electroactive molecule. This is a quite reasonable value, which indicates sub-monolayer coverage of the electrode surface by the enzyme (≥ 1 pmol cm^{-2} of the accessible electrode area) taking into account a real surface area of *ca.* 200 m^2 g^{-1}, as specified by the CNP provider (*vide supra*), and the real size of the enzyme from recently published crystal structures of *Mv*BOx [37, 38].

The differences between E_{mp} (mid-point potential) for low- and high-potential non-turnover signals, plotted in terms of ΔG ($\Delta G_{T1\to T23} = -n\Delta E_{T23\text{-}T1}$), were pH dependent (Fig. 3B, insert). From a comparison of voltammograms under aerobic and anaerobic conditions, one can conclude that the redox transformations observed in the absence of O_2 are directly connected to the two waves of bioelectrocatalysis, *i.e.* the first cathodic wave corresponds to a high-redox-potential non-catalytic process, whereas the second catalytic wave is related to the low-redox-potential non-turnover process (*cf.* Figs. 2 and 3A). In contrast to the starting potentials of O_2 bioelectroreduction, E_{mp} values for the non-catalytic Faradaic signals of BOx change by 0.023 and 0.057 V/pH-unit for the high- and low-redox-potential processes, respectively (Fig. 3B). The first value, which coincide with E_{T1} of the enzymes, also compares well to previously estimated pH dependences of E_{T1} of MCO, ~0.02 V/pH [78, 79]. Contrary to E_{T1}, the redox transformation of the Cu-T23 cluster should involve H^+ transfer. For such a process, a pH-dependence equal to 0.059 V/pH is predicted [81], and indeed such a dependence was obtained for the low-redox-potential non-turnover signal in Fig. 3B, which is attributed to E_{T23}. It is important to emphasize that the pH dependences of E_{mp} for the low- and high-potential non-turnover signals coincided with the pH dependences of half-wave potentials of low- and high-potential catalytic waves: 0.057 and 0.051 V/pH for the non-turnover and turnover signals of the low-potential processes, and 0.023 and 0.025 V/pH for the corresponding high-potential processes (*cf.* insert in Fig. 2B and Fig. 3B). Thus, the low- and high-redox-potential non-catalytic electrochemical signals are most likely related to the redox transitions of the Cu-T23 cluster and the Cu-T1 site, respectively. The half-wave potentials of the low- and high-potential catalytic waves were determined from the peaks on the first derivatives of linear sweep voltammogram (LSVs) of *Mv*BOx-based CPGCE recorded at different pH values (SI1, Fig. S5).

Third, when F^-, a known inhibitor of the active enzyme, was added to the O_2-saturated solution at 10–100 mM concentration, biocatalytic current densities from *Mv*BOx-based CPGCE were drastically reduced (SI1, Fig. S6). In contrast, larger ions related to the buffer contents had little effect on either current densities or shapes of CVs of BOD-modified carbon electrodes, both SPGE and CPGCE. In the

presence of fluoride ions, which bind to the Cu-T23 cluster of MCO [11], E_{mp} for the low-redox-potential non-turnover signal of *Mv*BOx decreased (SI1, Fig. S6B). Such behavior is in agreement with previously published data showing that F^- affects E_{T2} and E_{T3} of Lc, whereas the E_{T1} does not change [74].

Fourth, the stability of the two bioelectrocatalytic waves was evaluated at different pH values. Successive LSVs from *Mv*BOx-modified CPGCE over a one-hour period showed quite fast decrease in magnitude of the total bioelectrocatalytic response, especially at very acidic solutions, *e.g.* at pH 3.2 (SI1, Fig. S7). At that pH the enzyme is much less stable, compared to the neutral and alkaline solutions (Fig. 4A). However, no detectable changes in shape or feature positions in the catalytic waveform were noted, suggesting the presence of a single form of electrocatalytically active BOx on the electrode surface (SI1, Fig. S7); the population of which decreases over the time of the experiment, without formation of new species that contribute to the voltammetric response [82].

It is important to emphasize that contrary to the averaged bioelectrocatalytic activities of *Mv*BOx expressed in k_{cat} (Fig. 5, black-and-white curve 1), which were calculated from j_{cat} values (*vide infra*) obtained from LSVs recorded using several *Mv*BOx-CPGCEs (for each pH value, three different electrodes were studied to calculate k_{cat} deviation), a single biomodified electrode was employed to obtain the pH dependence presented in Fig. 4A. For this purpose a 50 mM NaH_2PO_4 solution was titrated with either NaOH or H_2SO_4 to get different pH values. An almost linear dependence of the bioelectrocatalytic activity of *Mv*BOx on solution pH was observed in neutral and alkaline solutions, *i.e.* from pH 7 and higher (Fig. 4A). In acidic media, however, clear deactivation of the enzyme was registered, *viz.* irreversible inactivation in the very acidic region (pH below 3.2) and reversible inhibition of the adsorbed *Mv*BOx in the pH range 3.2–4.2 (Fig. 4A, insert).

Finally, investigations of the activity of adsorbed *Mv*BOx on solution pH were performed at different O_2 concentrations, *viz.* in air and oxygen saturated solutions (Fig. 4B). Whereas in acidic solutions BOx followed typical Michaelis kinetic for enzymatic O_2 reduction, almost no difference in bioelectrocatalytic current densities was registered in the alkaline region (pH 8.1), when the O_2 concentration was changed from 0.25 mM to 1.2 mM (Fig. 4B), pointing to the fact that IET process starts to be the rate-limiting step of BOx function in alkaline solutions or, in other words, confirming that $k_2 < k_1$ and k_3 (Fig. 4B, insert) at least at pH 8.1 (*vide infra*).

3.3. Bioelectrocatalytic mechanism

The mechanism for the bioelectrocatalytic activity of MCO immobilized on different electrodes has recently been discussed in detail [16, 38]. The simplified scheme in Fig. 4B (insert) includes both interfacial and IET steps (processes 1 and 2 in Fig. 1), however, without a possibility to address several Cu centers of MCO simultaneously (*vide infra*). Nevertheless, this bioelectrocatalytic mechanism gives

a formal rationale for the observed apparent Michaelis–Menten kinetics of different MCOs, including BOx in previous [16, 38] and the present studies (Fig. 4B and Fig. S1 in SI1). Whereas processes 1 and 2 are in general reversible (Fig. 4B, insert), the reduction of O_2 by Cu-T23 is an irreversible step (k_3). It was demonstrated experimentally that at least one of the steps comprising the transformations of the Cu-T23 cluster, namely the oxidation of fully reduced Lc by O_2 with concomitant formation of the so-called peroxy intermediate, **PI** [20, 83], is a proton-independent, essentially irreversible, and very fast process [8, 10]. Since the Michaelis constant of BOx towards O_2, $K_M(O_2)$, depends on the potential, different rate-determining steps (heterogeneous ET and IET, *i.e.* k_1 and k_2) do exist in different potential regions, *i.e.* at low and high overpotentials.

Bioelectrocatalytic current densities from BOx-modified electrodes, when limited by the kinetics of the enzyme, can be calculated using the following equation:

$$j_{cat} = nFk_{cat}\Gamma C_{oxygen}/(C_{oxygen} + K_M(O_2)) \quad (7)$$

where j_{cat} is the bioelectrocatalytic current density, n the number of electrons participating in O_2 electroreduction, F Faraday constant, k_{cat} the catalytic constant of the enzyme in adsorbed state, Γ the enzyme concentration on the electrode surface, and C_{oxygen} the concentration of O_2 in solution.

Taking into account the K_M value for adsorbed BOx determined in our studies (~0.2 mM), calculations based on Eq. 7 imply that j_{cat} in O_2-saturated solutions should be 1.54 times higher than in air-saturated buffers, if the bioelectrocatalytic current densities from the BOx-modified electrodes were mostly limited by the kinetics of the enzyme. In spite of the well-pronounced dependence of j_{cat} on the applied potential, ratios of j_{cat} from *Mv*BOx-modified CPGCE submerged in air- and oxygen-saturated buffers close to 1.54 were obtained at pH 3.5 and 5.7, *viz.* 1.43 and 1.44, respectively (Fig. 4B). However, at pH 8.1, the j_{cat} ratio was only 1.09, suggesting ET limitations in the performance of enzyme-modified electrodes in alkaline solutions. Taking into account the identical and high overpotentails used in our calculations (0.2 V was applied to *Mv*BOx-modified CPGCE to register j_{cat} at different pH values) and drawing on the detailed mathematical description of the bioelectrocatalytic mechanism in Ref. [40], one can suggest that the IET process starts to be the rate-limiting step in alkaline solutions, *i.e.* $k_2 < k_1$ and k_3 and $k_2 \approx k_{cat}$.

Based on the maximal j_{cat} obtained in our studies (1 mA cm^{-2} at 0.1 V in O_2 saturated buffers pH 5) and other determined parameters (Γ, C_{oxygen}, and K_M), we were also able to calculate a minimal k_{cat} value for the adsorbed *Mv*BOx using Eq. 7. Taking into account the fact that $j_{cat} < j_{lim}$ (Fig. 2) one can conclude that $k_{cat} > 32\ s^{-1}$ for *Mv*BOx in heterogeneous catalysis of O_2 reduction.

3.4. Comparison of homogeneous and heterogeneous biocatalyses

Homogeneous and heterogeneous BOx-based catalysis was carefully investigated over a broad pH range (2.6–8.2). In Fig. 5 the observed k_{cat} values are plotted *vs.* pH. For the heterogeneous reduction of O_2 by *Mv*BOx, the pH dependence of the total electrocatalytic current from *Mv*BOx-modified CPGCE display bell-shaped profiles with the maximum at *ca.* pH 5 (Fig. 5, curve 1), in agreement with previously published results for *Mv*BOx immobilized on pyrolytic graphite 'edge' electrodes [16] submerged in solutions with pH ranging from 5 up to 8. For the homogeneous catalysis, similar pH dependences were also registered (*cf.* curves 1 and 2 in Fig. 5) for high-redox-potential, energy-poor substrates, *i.e.* $K_4[Mo(CN)_8]$ and ABTS (E_S = 0.78 V and 0.68 V, respectively; Table 1). However, for the low-redox-potential, energy-rich substrate ($K_4[Fe(CN)_6]$, E_S = 0.43 V), k_{cat} of BOx depended weakly on pH in the region 3.3–7.2, but the specific activity of the enzyme significantly dropped in buffer with pH 8.2 (Fig. 4A, curve 3).

It should be emphasized that it is very difficult to investigate BOx performance in very acidic solutions because of the fast deactivation of the enzyme, as was shown experimentally (Fig. 4A and Fig. S7 in SI1). It seems that several mechanisms might be involved in enzyme activity changes depending on solution pH: (*i*) irreversible BOx degradation in very acidic solutions (pH below 3.2), (*ii*) reversible enzyme inhibition close to the isoelectric point of the enzyme (pH 3.2–4.2), *i.e.* pI = 3.5 (SI1, Fig. S8), and (*iii*) above pH 6, the catalytic rate depends directly on the activity of H^+, evident by the linear correlation between BOx turnover numbers and solution pH. Thus, the decrease of observed k_{cat} and j_{cat} in both homogeneous and heterogeneous systems (Fig. 4A, curves 1 and 2; Fig. 4B; Table 1) in acidic solutions (pH 4 and below) reflect, in all likelihood, enzyme degradation rather than real changes of the specific activity of BOx.

On the one hand, turnover numbers of BOx do not significantly differ at pH below 6. Indeed, when the j_{cat} values are corrected with respect to enzyme degradation, taking into account the rate of this process at different pH values, almost no difference in the enzymatic activity measured at pH 3.5 and 5.7 was seen (Fig. 4B). A similar pH profile was also obtained using $K_4[Fe(CN)_6]$ as substrate (Fig. 5), possibly due to improved enzymatic stability in the absence of free radicals (*cf.* curves 2 and 3 in Fig. 5), which are formed during ABTS oxidation by MCO [84]. On the other hand, an almost linear correlation between k_{cat} and solution pH was observed in both the homogeneous and heterogeneous cases at pH 6 and higher (Fig. 4A, Fig. 5), again suggesting an IET rate-limiting step in alkaline solutions.

3.5. QM/MM calculations of reorganization energies

The experimental results described in the section 3.2 suggest that E_{T23} for the one of the catalytically relevant intermediates of the Cu cluster may be lower than E_{T1}, contrary to the common assumption [16, 29, 44]. To further elucidate this phenomenon, QM/MM calculations were performed to estimate the

reorganization energy (λ) associated with the electron transfer reactions involving the native intermediate, **NI**, which is assumed to be the catalytically competent fully oxidized intermediate [1, 9] in the MCO reaction cycle. Calculated λ values are listed in Tables 2 and 3 for both the Cu-T1 site and the Cu-T23 cluster.

The total λ is in the range 0.92–1.03 eV. Not surprisingly, the λ_1 values of the Cu-T1 site do not vary significantly (0.45–0.49 eV), because the QM region (system 1) is identical in all the calculations and the variations are only in the structure and total charge of the Cu-T23 cluster (as a part of the MM region, system 2). Interestingly, the same applies to the λ_2 values (0.47–0.54 eV).

For comparison, we also calculated λ for the reverse process, *i.e.* transfer of the electron from the T23 cluster to the T1 site, denoted λ'. As can be seen in Table 2, the λ_1' values are slightly lower than λ_1, whereas the λ_2' values are systematically higher (by ~0.4 eV) than λ_2 (Cu-T23 cluster). Thus, the overall λ' are 0.3–0.4 eV higher than λ.

In Table 3, we complemented these data by reorganization energies corresponding to the further reduction of the Cu-T23 cluster, *i.e.* to the process

$$T1^{(+)} + T23^{(5+)} \rightarrow T1^{(2+)} + T23^{(4+)} \quad (8)$$

for which the reorganization energy is denoted $\lambda_{(2\text{-el})}$. Based on the results and arguments given above, only the values of $\lambda_{(2\text{-el})}$ (reorganization energy of the Cu-T23 cluster after two electrons have been transferred) were calculated, assuming that the Cu-T1 λ_1 values are similar to those calculated for the first reduction. As can be seen in Table 3, the second reorganization energies for the Cu-T23 cluster are different from the reorganization energies corresponding to the first reduction. Therefore, the total $\lambda_{(2\text{-el})}$ are slightly higher (0.03–0.1 eV) than the λ values (*cf.* λ and $\lambda_{(2\text{-el})}$ in Tables 2 and 3, respectively).

3.5. State of the enzyme

The catalytic waves and non-turnover signals presented in Figs. 2 and 3 are central to our analysis of the BOx catalysis mechanism, provided that the BOx structure and function are not degraded on immobilization. Fortunately, there is ample evidence that BOx is not significantly damaged or degraded by surface adsorption.

First, the significant difference in current densities under air- and O_2-saturated conditions in acidic solutions clearly indicates that the catalytic current was related to the reduction of O_2 on the BOx-modified electrode surface (Figs. 2 and 3, Fig. 4B, and Fig. S1 in SI1). Moreover, similar $K_M(O_2)$ values (~0.2 mM) were estimated for homogeneous and heterogeneous biocatalyses. Importantly, the K_M value calculated in the heterogeneous system strongly depended on the potential applied to *Mv*BOx-modified

CPGCE, in agreement with the results for fungal BOx [16] and Lc [15]. Furthermore, the K_M value of Lc towards O_2 previously determined in homogeneous solution and bioelectrocatalytic studies was in the same concentration range (0.1–0.4 mM) [11, 15, 74, 75]. These facts suggest that BOx preserves the native state after adsorption on carbon materials.

Second, F^-, a well-know inhibitor of the enzyme, significantly depressed the electrocatalytic currents (SI1, Fig. S6), whereas larger ions related to the buffer contents had very little effect on either the current densities or the shapes of voltammograms of BOx-modified electrodes.

Third, when adsorbed on SPGE and CPGCE, two different enzymes, *Tt*BOx and *Mv*BOx, showed very similar electrochemical behavior (*cf.* Figs. 2A and 2B). Importantly, the complex shape of voltammograms and the presence of two bioelectrocatalytic processes starting at low and high potentials did not depend on the type of the electrode or on the source of BOx.

Finally, comparing the activity of *Mv*BOx in homogeneous and heterogeneous catalyses (Fig. 5), *e.g.* comparing observed k_{cat} values at pH 5, which are in the range of 46–121 s^{-1} for the enzyme in solution (Table 1) and > 32 s^{-1} in the adsorbed state (*vide supra*), we can conclude that BOx immobilized on carbon electrodes is at least quasi-native and definitely electrocatalytically active.

3.6. General discussion

Two bioelectrocatalytic waves on voltammograms of BOx-modified carbon electrodes can be explained using several hypotheses. One explanation is the presence of two catalytically active fractions of BOx with different E_{T1}, *e.g.* a fully active BOx and a partly denaturated enzyme, or two isoforms of BOx. However, as stated in the Experimental Section, both preparations were highly purified and one of them (*Tt*BOx) was homogeneous as judged from both SDS-PAGE and mass spectrometry. Moreover, the shapes and positions of features in the catalytic waveform did not depend on the source of BOx. Therefore, we consider it unlikely that two purified preparations obtained from two unrelated fungi, one ascomycete and one basidiomycete, have two identical catalytically active fractions of BOx. These arguments are further corroborated by the fact that the observed rates of degradation for both bioelectrocatalytic waves were very similar (SI1, Fig. S7).

Another explanation is the possible degradation of BOx on the electrode surface with the formation of two adsorbed fractions, *viz.* damaged and native ones with low- and high-redox-potentials, respectively, both in DET contact by the Cu-T1 site (Fig. 1B, right upper part). Such a considerable shift of E_{T1} could be possible only if the enzyme acquires a dramatically changed (denatured) conformation at the carbon surface. However, well-pronounced bioelectrocatalytic activities from both redox potentials were always registered in our studies. Moreover, it is quite improbable that for two different BOx (*Tt*BOx and *Mv*BOx) and two different carbon surfaces (SPGE and CPGCE), identical denaturation processes would be observed without the formation of partly denaturated fractions of the

enzyme. In the latter case, the heterogeneity in the interfacial electron transfer rates would imply that two well-pronounced bioelectrocatalytic waves cannot be obtained [85]. Furthermore, as discussed above, there is ample evidence that BOx is not significantly damaged or degraded by surface adsorption. Finally, the stability test of *Mv*BOx-modified CPGCE at different pH values is a strong evidence for a single form of electrochemically active enzyme on the electrode surface [82]. Taking also into account the different pH dependences obtained for low- and high-potential processes, when both non-turnover and turnover signals were evaluated (Fig. 2B, insert and Fig. 3B), we can safely reject these two explanations.

Thus, the third and most likely hypothesis, which is in good agreement with previously published data concerning electrochemical studies of different multicenter redox enzymes, is based on the possibility to address several redox centers of complex oxidoreductases simultaneously, *i.e.* in the case of BOx to electrically connect both the Cu-T1 and Cu-T23 sites of the enzyme. An analogy has been already reported for different FeS clusters in fumarate reductase [86] and different heme centers of cytochrome *c* nitrite reductase [82]. The exact mechanism of simultaneous electronic connection to several redox centers in complex enzymes is still a matter of debate [5, 82, 86]. A reasonable suggestion is the presence of a single form of electrochemically active BOx on the electrode surface, but in two different orientations with the Cu-T1 site and Cu-T23 cluster in DET contact (Fig. 1, right part), as was proposed in previous studies [5, 17, 23, 29]. This suggestion also coincides with recently published data concerning crystal structures of *Mv*BOx [37, 38]. It was shown that both the Cu-T1 site and the Cu-T23 cluster lie sufficiently close to the surface of the enzyme (< 14 Å) for DET at biologically relevant rates [38].

Thus, one can conclude that the first bioelectrocatalytic process (Fig. 2, E_{T1}) starts at quite high potentials and it is related to the Cu-T1 site of BOx (Fig. 1, right part). In contrast, the second bioelectrocatalytic process starts in the low-potential region (Fig. 2, E_{T23}) and we suggest that it is connected to the activity of the Cu-T23 cluster, which can have different E_{T23} values, including low-redox-potential intermediates, when the TNC is partly reduced, and high-redox-potential intermediates, such as the native and peroxy intermediates (**NI** and **PI**, respectively).

An important question is why a non-turnover Faradaic signal of the Cu-T23 cluster would be correlated to the low-redox-potential bioelectrocatalytic process. In other words, why was one of the E_{T23} values found to be the same under both aerobic and anaerobic conditions? To clarify the situation we begin by discussing the thermodynamic aspects of the biocatalytic process presented in Fig. 1, left part.

One of the basic parameters of an enzymatically catalyzed redox reaction is the difference in the standard redox potentials of the initial electron donor, the bridge (enzyme), and the final electron

acceptor. Accordingly, information about E_{T1} and E_{T23} values is needed to understand the redox reactions in the catalytic turnover of BOx.

In spite of the fact that only one E_{T1} value should exist as discussed above, it may be affected by the state of the Cu-T23 cluster and this effect may exceed 0.2 V according to our preliminary calculations [55]. Nevertheless, for this electron-relay center, a redox titration performed under anaerobic conditions should yield the catalytically relevant E_{T1} value. Importantly, it is widely held that in homogeneous catalysis, the ET rate between substrates and the Cu-T1 site (Fig. 1, left part) is a major factor determining the catalytic rate of the MCO due to a strong direct correlation of catalytic activity with the difference in the thermodynamic driving force ($\Delta G_{S\rightarrow T1}$) between the substrate and the Cu-T1 site of different MCO [50, 71, 72], including BOx for a series of substrates (Table 1).

The E_{T23} values are much more challenging to ascertain. Taking into account the many intermediates of MCO described in the literature (**NI**, **PI**, fully reduced enzyme (**Red**), and oxidized resting form, **Ox**), which have different structures of the Cu-T23 cluster [1, 9, 13, 14, 20], at least four E_{T23} values can be expected. Moreover, when **NI** is transformed to the **Red** three IET steps occur, so at least two intermediates with partly reduced Cu-T23 cluster with unknown structures are expected. As was mentioned in the Introduction, E_{T23} values are difficult to estimate by traditional potentiometric methods due to several reasons. Thus, below we attempt to shed light on the catalytically relevant E_{T1} and E_{T23} values of BOx and possibly for other MCO as well.

The physiologically relevant reaction catalyzed by BOx (Fig. 1, left part) is the oxidation of BR to BV, which is known to be a complicated pH-dependent high-potential redox reaction [87, 88]. Upon electrooxidation, BR is oxidized to BV at a potential of ~0.75 V [88]. Moreover, in the present studies efficient biocatalyitc oxidation of high-redox-potential compounds, *i.e.* ABTS and $K_4[Fe(CN)_8]$, was also shown (Table 1). Thus, E_{T1} of BOx, the first electron acceptor in the homogenous catalysis (Fig. 1, left part), should be relatively high in order to efficiently oxidize the natural substrate of the enzyme. Indeed, E_{T1} *value*s of *Mv*BOx and *Tt*BOx were measured to be ~0.7 V [18, 19].

As was previously suggested, one of the E_{T23} *value*s of MCO in general [6, 23], and of BOx in particular [5, 19], might be close to 0.4 V. Indeed, a redox transformation of BOx with E_{mp} ~0.4 V was also observed in the present studies with a pH dependence of 0.059 V/pH-unit (Fig. 3). Furthermore, this E_{T23} value correlates well with the second sigmoidal catalytic wave that appeared in the voltammograms of BOx-modified electrodes (*cf.* Figs. 2 and 3A). These results suggest that a redox intermediate of BOx with an E_{T23} value of ~0.4 V is catalytically active. It should be emphasized that the partly reduced intermediates should have lower E_{T23} values than the **PI** and **NI**, which are highly reactive and also likely to be strongly oxidizing [9, 16, 20]. Unfortunately, neither structures nor properties of partly reduced intermediates are known so far. Nevertheless, according to the catalytic cycle of MCO presented in the review by Solomon and co-workers [1], the redox transformation

between the first and second partly reduced Cu-T23 intermediates (Eq. 9) is a proton-dependent reaction that does not involve O_2 (Fig. 35 in Ref. [1]). This is in accordance with our results showing that the redox transformation of the Cu-T23 cluster observed in our electrochemical studies under both aerobic and anaerobic conditions (Figs. 2 and 3) is O_2-independent and H^+-dependent.

$$T23^{(5+)}\text{-OH} + H^+ + e^- \rightarrow T23^{(4+)} + H_2O \quad (9)$$

The two catalytically relevant E_{T1} and E_{T23} values of 0.7 V and 0.4 V (pH 7), respectively, indicate that at least one of the IET steps during the catalytic turnover of BOx is uphill, as suggested before [5]. In biological redox chains, the ET rate is determined by the redox potential difference between the donor and acceptor, their orbital overlap (electronic coupling), and the Frank–Condon barrier, *i.e.* the reorganization energy associated with the ET, λ [89]. Many biological ET chains contain an uphill ET step, and it has been hypothesized that this feature ensures that individual ET rates do not have to be optimized [90]. Approximate IET rates can be calculated from a simple empirical expression that incorporates an exponential decay of the tunneling rate with the edge-to-edge distance (R) and a parabolic dependence of the log rate of the IET on ΔG (for MCO $\Delta G_{T1\rightarrow T23} = -nF(E_{T23} - E_{T1})$) and λ [90, 91]:

$$\log(k_{IET}) = 15 - 0.6R - 3.1[(\Delta G + \lambda)^2/\lambda] \quad (10)$$

At a 13 Å distance (the approximate distance between Cu-T1 and Cu-T23 in MCOs in general [1] and BOx in particular {Mizutani, 2010 #558; Cracknell, 2011 #561}) and using the λ values of the IET presented in Tables 2 and 3, k_{IET} values are plotted as a function of pH in Fig. 5 (solid colored lines), based on the $\Delta G_{T1\rightarrow T23}$ values from Fig. 3B. Taking into account the overall errors in the calculated λ *value*s, one can conclude that the calculated k_{IET} values (from 3 s^{-1} up to 138 s^{-1} and higher) coincide quite well with turnover rates of BOx measured in both heterogeneous and homogeneous catalyses (Fig. 5, curves 1–3).

Two things are worthwhile to mention. First, the experimentally observed range of k_{IET} can be reproduced only for positive values ΔG. Already for ΔG = 0 eV, the calculated k_{IET} values are 10^3 s^{-1} or larger for λ = 0.92–1.39 eV, *i.e.* at least ten times large than observed experimentally. Second, the IET rate changes might be connected not only to the pH dependence of ΔG (which has, in a real system, a very complicated pattern because of many different intermediates of MCO formed during the catalytic cycle and since E_{T1} depends on E_{T23} and *vice versa* {Hu, 2011 #576}), but also to the not yet investigated pH dependence of λ_{IET}, since both λ_1 and λ_2 should be pH-dependent as already proved for

the Cu-T1 site [92]. Nevertheless, calculated k_{IET} using λ values (0.92–1.13 eV) for the forward IET process (T1→T23) are in good agreement with measured k_{cat} in alkaline solutions (Fig. 5).

Thus, based on our experimental and theoretical results we conclude that the IET rate can become the rate-limiting step in biocatalytic reduction of O_2 by BOx under certain conditions (pH above 7), enabling straight correlation between BOx turnover numbers and solution pH because of E_{T23} 0.057 V/pH dependence. For this to occur, both k_1 and $k_3 > k_2$ (Fig. 4B, insert), or in other words, the rates of processes 1 and 3 (Fig. 1) should be considerably higher than the rate of process 2 (IET, Fig. 1). We now analyze these processes in turn.

Let us first consider the rate at which O_2 interacts with the Cu cluster and is converted to H_2O (process 3 in Fig. 1; k_3 in Fig. 4B, insert). In the literature, the second-order rate constant for the oxidation of the Cu-T23 cluster in Lc by O_2 is available, *viz.* ~10^7 M^{-1} s^{-1} at 25°C and pH 7.4 [7, 8, 10]. The K_M values of different Lc towards O_2 in homogeneous solution and in the adsorbed state are similar, 0.1–0.5 mM [11, 15, 74, 75] and coincide well with the K_M values of *Mv*BOx determined in both homogeneous and heterogeneous biocatalyses, ~0.2 mM (*vide supra*). The fact that Lc and BOx have similar $K_M(O_2)$ values and an almost identical ligand pattern of the T2 and T3 copper ions shows the strong structural and kinetic similarity of the two enzymes, and indicates that the second-order rate constant of O_2 reduction by the Cu-T23 cluster of Lc is also likely to be valid for BOx. Consequently, the theoretical rate of O_2 reduction by the Cu-T23 cluster of BOx can be as high as $2.6 \cdot 10^3$ s^{-1} under air-saturated conditions. Such a rate is fast enough not to limit the overall turnover rate (k_{cat} = 22–138 s^{-1} for typical substrates according to the results in Table 1 and >32 s^{-1} for heterogeneous bioelectrocatalysis), and indicates that O_2 penetration to reach the Cu-T23 cluster of BOx and the formation of the enzyme-O_2 adducts are fast processes. Thus, the determination of the kinetic parameters of O_2 reduction by the Cu-T23 cluster of MCO in a homogeneous assay is quite difficult because the turnover rate usually tends to be limited by the oxidation of substrates at the T1 pocket of the MCO [3, 71, 93].

There is no information, however, concerning the rate of H_2O release from the Cu-T23 cluster of MCO. As early as in 1998, it was suggested that this process might be the rate-determining step during bioelectrocatalytic reduction of O_2 by Lc based on detailed bioelectrochemical studies of an adsorbed high-redox-potential enzyme from the basidiomycete *Trametes versicolor* [15]. Indeed, we cannot disregard this possibility for BOx biocatalytic reactions in acidic solutions, *e.g.* in the case of the high k_{cat} values obtained for low-redox-potential substrates and heterogeneous bioelectrocatalysis at high overpotentials.

Let us now consider the supply of an electron to the Cu-T1 site (process 1 in Fig. 1; k_1 in Fig. 4B, insert). The MCO substrates can in principle be divided in two groups: electron–proton donors and electron–only donors [71, 72, 94]. The first group includes phenols and aromatic amines, for which the

formal potentials strongly depend on the solution pH. It is widely held that the bell-shaped activity–pH profile of MCOs is caused two simultaneous processes, *viz.* inhibition of enzymes by OH^- at alkaline pH and a decrease in the thermodynamic driving force ($\Delta E_{T1\text{-}S}$) at acidic pH [71, 72, 94]. The second group includes simple inorganic redox compounds, *e.g.* $K_4[Fe(CN)_6]$ and $K_4[Mo(CN)_8]$, and organic substrates, which are oxidized by MCO through a radical mechanism, *e.g.* ABTS [95]. For these substrates, a decrease in MCO activity at high pH is usually observed, which is explained by the inhibition of the enzyme by OH^- [1, 50]. It should be emphasized that substrates from the second group were used in our studies and one could expect a linear dependence of BOx activity on solution pH. Nevertheless, quite complex pH profiles for the substrates were obtained (Fig. 5, curves 2 and 3; Table 1), which might be connected to the deactivation of the enzyme in acidic solutions as already discussed above.

In homogeneous catalysis, the low-redox-potential inorganic substrate, $K_4[Fe(CN)_6]$ has the highest k_{cat} value yet observed among all known BOx substrates [4, 47, 72, 73, 96], up to 138 s^{-1} (Table 1). However, even for $K_4[Fe(CN)_6]$ (with E_s = 0.43 V or $\Delta G_{S\to T1}$ = –0.27 eV), the measured k_{cat} value was still dramatically lower than the maximum possible rate of O_2 reduction by the Cu-T23 cluster (*vide supra*). As expected, k_{cat} of BOx for $K_4[Mo(CN)_8]$ and ABTS, substrates with higher redox potentials, were much lower than the value obtained for $K_4[Fe(CN)_6]$ (Table 1). Thus, during the physiologically relevant biocatalytic reaction (Fig. 1, left part), the specific activity of BOx, in all likelihood, depends on the rate of BR oxidation (E_s = 0.75 V) at the Cu-T1 site of the enzyme. However, in heterogeneous biocatalytic reactions of O_2 reductions (Fig. 1, right part), widely used in biofuel cells nowadays (*e.g.* Refs. [32-36]), as well as in homogeneous catalysis under certain conditions, *e.g.* at pH 7 and higher, the IET process might be the rate-limiting step determining the ultimate efficiency of BOx-based biocatalysis.

If our model of BOx function is correct, *i.e.* if the IET is the rate-determining step, it should be possible to engineer BOx so that the limiting IET rate will be easier to observe. This has also been done. For example, a significant increase of k_{cat} for a T1-site-mutated (Met467Gln) *Mv*BOx was obtained (E_{T1} = 0.43 V; $\Delta G_{S\to T1}$ = 0 eV; k_{cat} = 579 s^{-1}) compared to the wild-type enzyme (E_{T1} = 0.67 V; $\Delta G_{S\to T1}$ = –0.24 eV; k_{cat} = 393 s^{-1}), whereas the $K_M(O_2)$ values were quite similar for the mutant and wild-type enzymes (~0.11 mM) during the homogeneous oxidation of $K_4[Fe(CN)_6]$ [73]. At the same time, the activity of the enzyme towards the natural substrate BR was abolished by the same mutation, most likely because $\Delta G_{S\to T1}$ becomes too positive (+0.32 eV). Obviously, when the IET is not a limiting step, but substrate oxidation limits the rate of biocatalytic reaction, a significant decrease in E_{T1} from 0.67 V to 0.43 V should decrease the observed k_{cat} values since the oxidative activity of the Cu-T1 was dropped. However, opposite result was obtained for mutated BOx [73]. Moreover, a significant increase of the catalytic turnover of *Mv*BOx during heterogeneous bioelectroreduction of O_2 was observed when

E_{T1} of the enzyme was decreased from 0.67 to 0.43 V by site-directed mutagenesis [44]. In addition to the explanation presented by the authors of Refs. [44, 73], we believe that their results can be also interpreted in terms of a decreased $\Delta G_{T1\rightarrow T23}$ for the IET reaction between the Cu-T1 site and the Cu-T23 copper cluster, thus supporting our main conclusion about the existence of a rate-limiting IET uphill step.

An uphill and overall relatively slow IET process might be also responsible for inhibition of BOx by anions (OH^- and F^-), which interact with the Cu-T23 cluster [11, 12, 17, 41] and decrease E_{T23} values, but do not affect on the affinity of the Cu cluster towards O_2 [11, 46]. The slow IET might also be responsible for slow formation of different resting forms of the enzyme [1, 9, 13, 14] due to spontaneous changes of the cluster with concomitant reduction of E_{T23}. Even if oxidation level of the Cu ions in the **Ox** and **NI** states of the enzyme are identical, the redox potentials of these intermediates are not necessarily close because the cluster geometry and ligand environment may be quite different. One can also speculate about the possible role of the slow IET as an important factor in regulating the activity of high-redox-potential MCO (in addition to the regulation by substrate specificity [3, 93]).

4. Conclusions

Kinetic and electrochemical properties of *Trachyderma tsunodae* and *Myrothecium verrucaria* BOx have been studied experimentally. The previous studies of Box were extended by carrying out investigations in broad potential (0–1.0 V) and pH (2.6–8.2) ranges using pure enzyme preparations. Our main conclusion is that an IET process can be the rate-limiting step under certain conditions, *e.g.* in alkaline solution, and that the BOx catalytic rate is not always limited by the rate of substrate oxidation at the Cu-T1 site. It was electrochemically shown that one of the catalytically relevant intermediates formed during the catalytic cycle of BOx might have a low redox potential close to 0.4 V at pH 7 (with a pH dependence of 0.057 V/pH), indicating an uphill IET process from the Cu-T1 site (with E_{T1} ~0.7 V) to the Cu-T23 cluster of BOx. Thus, we conjecture that the slow rate-limiting IET transfer occurs because of the uphill IET process.

This novel and interesting alternative hypothesis broadening our understanding of the catalytic action of this important family of the enzymes, was corroborated by combined QM/MM calculations of the reorganization energies for the ET from the Cu-T1 site to the Cu-T23 cluster. Several states of the Cu-T23 cluster were considered and the calculations showed that the reorganization energies are 0.42–0.49 eV for the Cu-T1 site and 0.40–0.97 eV for the Cu-T23 cluster. Calculations of the IET rate, based on the experimentally observed Gibbs free energy change and theoretical estimates of reorganization energy obtained by combined QM/MM calculations, are compatible with the hypothesis that the uphill IET process is the rate-limiting step of BOx catalysis in alkaline solutions.

Acknowledgments. The authors thank Amano Enzyme Inc. for the kind gift of Amano 3 preparation of *M. verrucaria* bilirubin oxidase. The authors also thank Dr. Nicolas Mano and Dr. Olga V. Morozova for providing *T. tsunodae* and *M. verrucaria* bilirubin oxidases, respectively. The work has been supported financially by the European Commission (FP7 project NMP4-SL-2009-229255), and the Swedish Research Council (project 2009-3266).

Supporting Information Available. Part 1: Additional biochemical and electrochemical studies of two enzymes and two electrodes. Part 2: The structure of the whole protein used in QM/MM calculations (including the point charges on the atoms) and the structures (Cartesian coordinates) of all the quantum regions (S1 systems) used in this work. This material is available free of charge *via* the Internet.

References

[1] E. I. Solomon, U. M. Sundaram, T. E. Machonkin, *Chem. Rev.* **1996**, *96*, 2563.

[2] T. Sakurai, K. Kataoka, *Chem. Record* **2007**, *7*, 220.

[3] T. Sakurai, K. Kataoka, *Cell. Mol. Life Sci.* **2007**, *64*, 2642.

[4] S. Tsujimura, T. Nakagawa, K. Kano, T. Ikeda, *Electrochemistry (Tokyo)* **2004**, *72*, 437.

[5] P. Ramirez, N. Mano, R. Andreu, T. Ruzgas, A. Heller, L. Gorton, S. Shleev, *Biochim. Biophys. Acta* **2008**, *1777*, 1364.

[6] S. Shleev, J. Tkac, A. Christenson, T. Ruzgas, A. I. Yaropolov, J. W. Whittaker, L. Gorton, *Biosens. Bioelectron.* **2005**, *20*, 2517.

[7] L. E. Andreasson, B. Reinhammar, *Biochim. Biophys. Acta* **1976**, *445*, 579.

[8] J. L. Cole, D. P. Ballou, E. I. Solomon, *J. Am. Chem. Soc.* **1991**, *113*, 8544.

[9] S.-K. Lee, S. DeBeer George, W. E. Antholine, B. Hedman, K. O. Hodgson, E. I. Solomon, *J. Am. Chem. Soc.* **2002**, *124*, 6180.

[10] I. Matijosyte, I. W. C. E. Arends, R. A. Sheldon, S. de Vries, *Inorg. Chim. Acta* **2008**, *361*, 1202.

[11] A. Naqui, S. D. Varfolomeev, *FEBS Lett.* **1980**, *113*, 157.

[12] J. Hirose, K. Inoue, H. Sakuragi, M. Kikkawa, M. Minakami, T. Morikawa, H. Iwamoto, K. Hiromi, *Inorg. Chim. Acta* **1998**, *273*, 204.

[13] T. Sakurai, L. Zhan, T. Fujita, K. Kataoka, A. Shimizu, T. Samejima, S. Yamaguchi, *Biosci. Biotechnol. Biochem.* **2003**, *67*, 1157.

[14] S. Shleev, C. T. Reimann, V. Serezhenkov, D. Burbaev, A. I. Yaropolov, L. Gorton, T. Ruzgas, *Biochimie* **2006**, *88*, 1275.

[15] M. H. Thuesen, O. Farver, B. Reinhammar, J. Ulstrup, *Acta Chem. Scand.* **1998**, *52*, 555.

[16] L. dos Santos, V. Climent, C. F. Blanford, F. A. Armstrong, *Phys. Chem. Chem. Phys.* **2010**, *12*, 13962.

[17] S. Shleev, T. Ruzgas, *Angew. Chem., Int. Ed.* **2008**, *47*, 7270.

[18] S. Tsujimura, A. Kuriyama, N. Fujieda, K. Kano, T. Ikeda, *Anal. Biochem.* **2005**, *337*, 325.

[19] A. Christenson, S. Shleev, N. Mano, A. Heller, L. Gorton, *Biochim. Biophys. Acta* **2006**, *1757*, 1634.

[20] L. Rulíšek, E. I. Solomon, U. Ryde, *Inorg. Chem.* **2005**, *44*, 5612.

[21] E. I. Solomon, M. J. Baldwin, M. D. Lowery, *Chem. Rev.* **1992**, *92*, 521.

[22] E. I. Solomon, R. K. Szilagyi, S. DeBeer George, L. Basumallick, *Chem. Rev.* **2004**, *104*, 419.

[23] S. Shleev, A. Christenson, V. Serezhenkov, D. Burbaev, A. Yaropolov, L. Gorton, T. Ruzgas, *Biochem. J.* **2005**, *385*, 745.

[24] K. H. Hyung, K. Y. Jun, H.-G. Hong, H. S. Kim, W. Shin, *Bull. Korean Chem. Soc.* **1997**, *18*, 564.

[25] M. Gelo-Pujic, H. H. Kim, N. G. Butlin, G. T. Palmore, *Appl. Environ. Microbiol.* **1999**, *65*, 5515.

[26] C.-J. Yoon, H.-H. Kim, *J. Korean Electrochem. Soc.* **2004**, *7*, 26.

[27] M. Pita, S. Shleev, T. Ruzgas, V. M. Fernandez, A. I. Yaropolov, L. Gorton, *Electrochem. Commun.* **2006**, *8*, 747.

[28] S. Shleev, M. Pita, A. I. Yaropolov, T. Ruzgas, L. Gorton, *Electroanalysis* **2006**, *18*, 1901.

[29] D. Ivnitski, P. Atanassov, *Electroanalysis* **2007**, *19*, 2307.

[30] M. E. Goldfinch, G. A. Maguire, *Ann. Clin. Biochem.* **1988**, *25*, 73.

[31] A. Westwood, *Ann. Clin. Biochem.* **1991**, *28*, 119.

[32] S. C. Barton, J. Gallaway, P. Atanassov, *Chem. Rev.* **2004**, *104*, 4867.

[33] A. Heller, *Phys. Chem. Chem. Phys.* **2004**, *6*, 209.

[34] I. Willner, Y. M. Yan, B. Willner, R. Tel-Vered, *Fuel Cells* **2009**, *9*, 7.

[35] R. Bilewicz, M. Opallo, *Fuel Cell Sci.* **2009**, 169.

[36] M. Falk, Z. Blum, S. Shleev, *Electrochimica Acta* **2012**, doi:10.1016/j.electacta.2011.12.133.

[37] K. Mizutani, M. Toyoda, K. Sagara, N. Takahashi, A. Sato, Y. Kamitaka, S. Tsujimura, Y. Nakanishi, T. Sugiura, S. Yamaguchi, K. Kano, B. Mikami, *Acta Crystallogr., Sect. F: Struct. Biol. Cryst. Commun.* **2010**, *F66*, 765.

[38] J. A. Cracknell, T. P. McNamara, E. D. Lowe, C. F. Blanford, *Dalton Trans.* **2011**, *40*, 6668.

[39] S. Shleev, A. El Kasmi, T. Ruzgas, L. Gorton, *Electrochem. Commun.* **2004**, *6*, 934.

[40] V. Climent, J. Zhang, E. P. Friis, L. H. Oestergaard, J. Ulstrup, *J. Phys. Chem. C* **2012**, *116*, 1232.

[41] L. E. Andreasson, B. Reinhammar, *Biochim. Biophys. Acta* **1979**, *568*, 145.

[42] J. Guo, X. X. Liang, P. S. Mo, G. X. Li, *Appl. Biochem. Biotechnol.* **1991**, *31*, 135.

[43] K. Hiromi, Y. Yamaguchi, Y. Sugiura, H. Iwamoto, J. Hirose, *Biosci. Biotechnol. Biochem.* **1992**, *56*, 1349.

[44] Y. Kamitaka, S. Tsujimura, K. Kataoka, T. Sakurai, T. Ikeda, K. Kano, *J. Electroanal. Chem.* **2007**, *601*, 119.

[45] A. Messerschmidt, Editor, *Multi-Copper Oxidases*, **1997**.

[46] A. Nagui, S. D. Varfolomeev, *Biokhimiya (Moscow)* **1981**, *46*, 1694.

[47] A. Shimizu, J. H. Kwon, T. Sasaki, T. Satoh, N. Sakurai, T. Sakurai, S. Yamaguchi, T. Samejima, *Biochemistry* **1999**, *38*, 3034.

[48] A. Shimizu, T. Samejima, S. Hirota, S. Yamaguchi, N. Sakurai, T. Sakurai, *J. Biochem. (Tokyo)* **2003**, *133*, 767.

[49] F. Xu, *J. Biol. Chem.* **1997**, *272*, 924.

[50] F. Xu, A. E. Palmer, D. S. Yaver, R. M. Berka, G. A. Gambetta, S. H. Brown, E. I. Solomon, *J. Biol. Chem.* **1999**, *274*, 12372.

[51] M. Srnec, U. Ryde, L. Rulíšek, *Faraday Discuss.* **2011**, *148*, 41.

[52] J. Chalupsky, F. Neese, E. I. Solomon, U. Ryde, L. Rulíšek, *Inorg. Chem.* **2006**, *45*, 11051.

[53] U. Ryde, Y.-W. Hsiao, L. Rulíšek, E. I. Solomon, *J. Am. Chem. Soc.* **2007**, *129*, 726.

[54] G. Hong, D. M. Ivnitski, G. R. Johnson, P. Atanassov, R. Pachter, *J. Am. Chem. Soc.* **2011**, *133*, 4802.

[55] L. Rulíšek, U. Ryde, *Coord. Chem. Rev.* **2012**, *in press*.

[56] B. Ehresmann, P. Imbault, J. H. Weil, *Anal. Biochem.* **1973**, *54*, 454.

[57] H. Jaegfeldt, T. Kuwana, G. Johansson, *J. Am. Chem. Soc.* **1983**, *105*, 1805.

[58] U. A. Paulus, T. J. Schmidt, H. A. Gasteiger, R. J. Behm, *J. Electroanal. Chem.* **2001**, *495*, 134.

[59] M. R. Tarasevich, G. V. Zhutaeva, V. A. Bogdanovskaya, M. V. Radina, M. R. Ehrenburg, A. E. Chalykh, *Electrochim. Acta* **2007**, *52*, 5108.

[60] U. Ryde, *J. Comput.-Aided Mol. Des.* **1996**, *10*, 153.

[61] U. Ryde, M. H. M. Olsson, *Inter. J. Quant. Chem.* **2001**, *81*, 335.

[62] O. Treutler, R. Ahlrichs, *J. Chem. Phys.* **1995**, *102*, 346.

[63] D. A. Case, T. E. Cheatham, III, T. Darden, H. Gohlke, R. Luo, K. M. Merz, Jr., A. Onufriev, C. Simmerling, B. Wang, R. J. Woods, *J. Comput. Chem.* **2005**, *26*, 1668.

[64] W. D. Cornell, P. Cieplak, C. I. Bayly, I. R. Gould, K. M. Merz, Jr., D. M. Ferguson, D. C. Spellmeyer, T. Fox, J. W. Caldwell, P. A. Kollman, *J. Am. Chem. Soc.* **1995**, *117*, 5179.

[65] J. P. Perdew, K. Burke, M. Ernzerhof, *Phys. Rev. Lett.* **1996**, *77*, 3865.

[66] K. Eichkorn, F. Weigend, O. Treutler, R. Ahlrichs, *Theor. Chem. Acc.* **1997**, *97*, 119.

[67] F. Weigend, R. Ahlrichs, *Phys. Chem. Chem. Phys.* **2005**, *7*, 3297.

[68] A. D. Becke, *J. Chem. Phys.* **1993**, *98*, 5648.

[69] S. A. Roberts, A. Weichsel, G. Grass, K. Thakali, J. T. Hazzard, G. Tollin, C. Rensing, W. R. Montfort, *Proc. Natl. Acad. Sci. U. S. A.* **2002**, *99*, 2766.

[70] L. H. Hu, M. Farrokhnia, J. Heimdal, S. Shleev, L. Rulíšek, U. Ryde, *J. Phys. Chem. B* **2011**, *115*, 13111.

[71] F. Xu, *Biochemistry* **1996**, *35*, 7608.

[72] F. Xu, W. Shin, S. H. Brown, J. A. Wahleithner, U. M. Sundaram, E. I. Solomon, *Biochim. Biophys. Acta* **1996**, *1292*, 303.

[73] A. Shimizu, T. Sasaki, J. H. Kwon, A. Odaka, T. Satoh, N. Sakurai, T. Sakurai, S. Yamaguchi, T. Samejima, *J. Biochem. (Tokyo)* **1999**, *125*, 662.

[74] B. R. M. Reinhammar, *Biochim. Biophys. Acta* **1972**, *275*, 245.

[75] E. Nazaruk, A. Michota, J. Bukowska, S. Shleev, L. Gorton, R. Bilewicz, *J. Biol. Inorg. Chem.* **2007**, *12*, 335.

[76] M. Weigel, E. Tritscher, F. Lisdat, *Electrochem. Commun.* **2007**, *9*, 689.

[77] D. Ivnitski, K. Artyushkova, P. Atanassov, *Bioelectrochemistry* **2008**, *74*, 101.

[78] T. Nakamura, *Biochimica et Biophysica Acta* **1958**, *30*, 44.

[79] S. Shleev, A. Jarosz-Wilkolazka, A. Khalunina, O. Morozova, A. Yaropolov, T. Ruzgas, L. Gorton, *Bioelectrochemistry* **2005**, *67*, 115.

[80] A. I. Yaropolov, A. N. Kharybin, J. Emneus, G. Marko-Varga, L. Gorton, *Bioelectrochem. Bioenerg.* **1996**, *40*, 49.

[81] A. J. Bard, L. R. Faulkner, *Electrochemical Methods: Fundamentals and Applications*, Wiley, New York, **1980**.

[82] H. C. Angove, J. A. Cole, D. J. Richardson, J. N. Butt, *J. Biol. Chem.* **2002**, *277*, 23374.

[83] J. Yoon, B. D. Liboiron, R. Sarangi, K. O. Hodgson, B. Hedman, E. I. Solomon, *Proc. Natl. Acad. Sci. USA* **2007**, *104*, 13609.

[84] R. Bourbonnais, D. Leech, M. G. Paice, *Biochim. Biophys. Acta* **1998**, *1379*, 381.

[85] C. Leger, A. K. Jones, S. P. J. Albracht, F. A. Armstrong, *J. Phys. Chem. B* **2002**, *106*, 13058.

[86] A. Sucheta, R. Cammack, J. Weiner, F. A. Armstrong, *Biochemistry* **1993**, *32*, 5455.

[87] G. Cheng, Y. Yang, S. Dong, *Bioelectrochem. Bioenerg.* **1991**, *26*, 345.

[88] G. Cheng, Y. Yang, S. Dong, *Bioelectrochem. Bioenerg.* **1994**, *34*, 141.

[89] R. A. Marcus, N. Sutin, *Biochim. Biophys. Acta* **1985**, *811*, 265.

[90] C. C. Page, C. C. Moser, X. Chen, P. L. Dutton, *Nature* **1999**, *402*, 47.

[91] C. C. Moser, P. L. Dutton, *Biochim. Biophys. Acta* **1992**, *1101*, 171.

[92] O. Farver, H. J. Hwang, Y. Lu, I. Pecht, *J. Phys. Chem. B* **2007**, *111*, 6690.

[93] L. Quintanar, C. Stoj, A. B. Taylor, P. J. Hart, D. J. Kosman, E. I. Solomon, *Acc. Chem. Res.* **2007**, *40*, 445.

[94] F. Xu, J. J. Kulys, K. Duke, K. Li, K. Krikstopaitis, H. J. Deussen, E. Abbate, V. Galinyte, P. Schneider, *Appl. Environ. Microbiol.* **2000**, *66*, 2052.

[95] R. Bourbonnais, D. Leech, M. G. Paice, *Biochimica et Biophysica Acta* **1998**, *1379*, 381.

[96] K. Kataoka, K. Tanaka, Y. Sakai, T. Sakurai, *Protein Expr. Purif.* **2005**, *41*, 77.

Tables

Table 1. Observed k_{cat} values (in sec^{-1}) of *Mv*BOx towards different substrates at different pH values (0.05 M universal buffer).

Substrate	E_S	$\Delta E_{T1\text{-}S}$	pH 3.3	pH 4.2	pH 5.2	pH 6.2	pH 7.2	pH 8.2
$K_4[Fe(CN)_6]$	0.43	0.27	131 ± 11	138 ± 11	121 ± 14	122 ± 4	114 ± 11	50 ±2
ABTS	0.68	0.02	22 ± 5	67 ± 3	73 ± 13	76 ± 3	63 ± 3	35 ± 1
$K_4[Mo(CN)_8]$	0.78	-0.08	45 ± 6	49 ± 5	46 ± 8	53 ± 2	46 ± 3	27 ± 2

Notes: E_S (redox potentials of substrates) are in V. The redox potential of ABTS is taken from Ref. [95]. For the calculation of $\Delta E_{T1\text{-}S}$, it was assumed that $E_{T1} = 0.7$ V.

Table 2. Calculated reorganization energies based on the structure of the NI. λ_1 and λ_2 (see Eqs. 5 and 6) are the reorganization energies of the Cu-T1 site and Cu-T23 clusters, respectively. λ and λ' are the reorganization energies for the forward (T1→T23) and the reverse (T23→T1) processes, respectively. All values are in eV.

State (QM/MM)	λ_1	λ_2	λ_1'	λ_2'	λ	λ'
$T23_{ox,red}$'/$T1_{red}$		0.54		0.90	1.03	1.34
$T1_{red,ox}$'/$T23_{ox}$	0.49		0.44			
$T23_{ox,red}$'/$T1_{ox}$		0.47		0.97	0.92	1.39
$T1_{red,ox}$'/$T23_{red}$	0.45		0.42			

Concerning nomenclature, $T1_{red,ox}$'/$T23_{ox}$ refers to the transition $T1^{1+}$→$T1^{2+}$ using optimized structure for $T23^{6+}$, for example.

Table 3. Calculated reorganization energies, where λ_1 (see Eq. 5) corresponds to the Cu-T1 site, $\lambda_{2(2\text{-el})}$ (see Eq. 7) corresponds to the second reduction of the Cu-T23 cluster, and $\lambda_{(2\text{-el})}$ corresponds to the IET process during the overall two-electron reduction of the Cu-T23 cluster. All values are in eV.

MM state	λ_1	$\lambda_{2(2\text{-el})}$	$\lambda_{(2\text{-el})}$
Cu-$T1_{red}$	0.49	0.64	1.13
Cu-$T1_{ox}$	0.45	0.50	0.95

Figure legends

Figure 1. Schematic representations of the physiologically relevant reactions catalyzed by BOx (left part) and the heterogeneous electroreduction of O_2 by the enzyme (right part). The structures of the model systems representing the Cu-T1 site and the Cu-T23 cluster of the native intermediate (NI) were also used in the QM/MM calculations as the Q1 and Q2 systems.

Figure 2. Typical voltammograms of BOx-modified carbon electrodes. The vertical lines represent the redox-potentials of the Cu-T1 site (E_{T1}) and one of the intermediate (the low-redox-potential intermediate) of the Cu-T23 cluster (E_{T23}). (A) LCVs of stationary *Tt*BOx-SPGE immersed in 0.05 M citrate-phosphate buffer pH 4.0 containing 0.1 mM $NaClO_4$ saturated with (1) N_2, (2) air, and (3) O_2. (B) LSVs of *Mv*BOx-CPGCE (200 μg cm^{-2} of CNP) in 0.05 M universal buffer pH 4.2 saturated with O_2. (1) stationary electrode without BOx, (2) stationary electrode with BOx, (3) rotating electrode (2000 rpm) with BOx. Insert: half-waves potential dependences of high- and low-potential bioelectrocatalytic processes on the solution pH.

Figure 3. (A) CVs of *Mv*BOx-CPGCE (200 μg cm^{-2} of CNP) under anaerobic conditions at different pH values. (B) E_{mp} dependences of high and low redox potential processes on the solution pH. Insert: ΔG dependence ($-n(E_{T23} - E_{T1})$; in eV) on the solution pH. Conditions: 0 rpm, 20 mV s^{-1}, 0.05 M universal buffer saturated with N_2.

Figure 4. The dependence of bioelectrocatalytic activity of *Mv*BOx-modified CPGCE on solution pH (A). Star – starting point of the titration, dotted line (open circles) – first direction of the titration from acidic (pH 3.2) to alkaline (pH 8.2) medium, solid line (open triangles) – second direction of the titration from alkaline (pH 8.2) to acidic (pH 3.2) medium, bold line (full squares) – third direction of the titration from very acidic (pH 2.8) directly to neutral (pH 6.2) medium. Insert: Typical chronoamperogram corresponding to the three initial points (open circles) of the first titration curve (dotted line) in the main figure. Conditions: 0.05 M air saturated NaH_2PO_4 adjusted with 1M NaOH or 0.5M H_2SO_4; the steady-state catalytic currents were measured at 0.2 V *vs.* NHE and corrected taking into consideration small mass transfer limitations. (B) The dependence on solution pH of the bioelectrocatalytic currents, corrected for enzyme degradation and recorded in air (open squares) or in oxygen-saturated 0.05 M universal buffer (full circles). Insert: simplified kinetic scheme of BOx-based bioelectrocatalytic systems.

Figure 5. Comparison of the dependences of the theoretically calculated k_{IET} and practically measured k_{cat} of *Mv*BOx on solution pH. k_{IET} – colored curves, k_{cat} – black-and-white curves. k_{IET} values were calculated from Eq. 10 using the ΔG values presented in Fig. 3B and a range of λ values (as indicated, in eV) from the QM/MM calculations in Tables 2 and 3. Curves 1, 2, and 3 (circles, squares, and triangles, respectively) correspond to homogeneous (2 – ABTS, 3 – $K_4[Fe(CN)_6]$; Table 1) and heterogeneous (curve 1; calculated based on Eq. 7) activities of *Mv*BOx expressed in k_{cat}. Conditions: 0.05 M universal buffer.

Figure 1

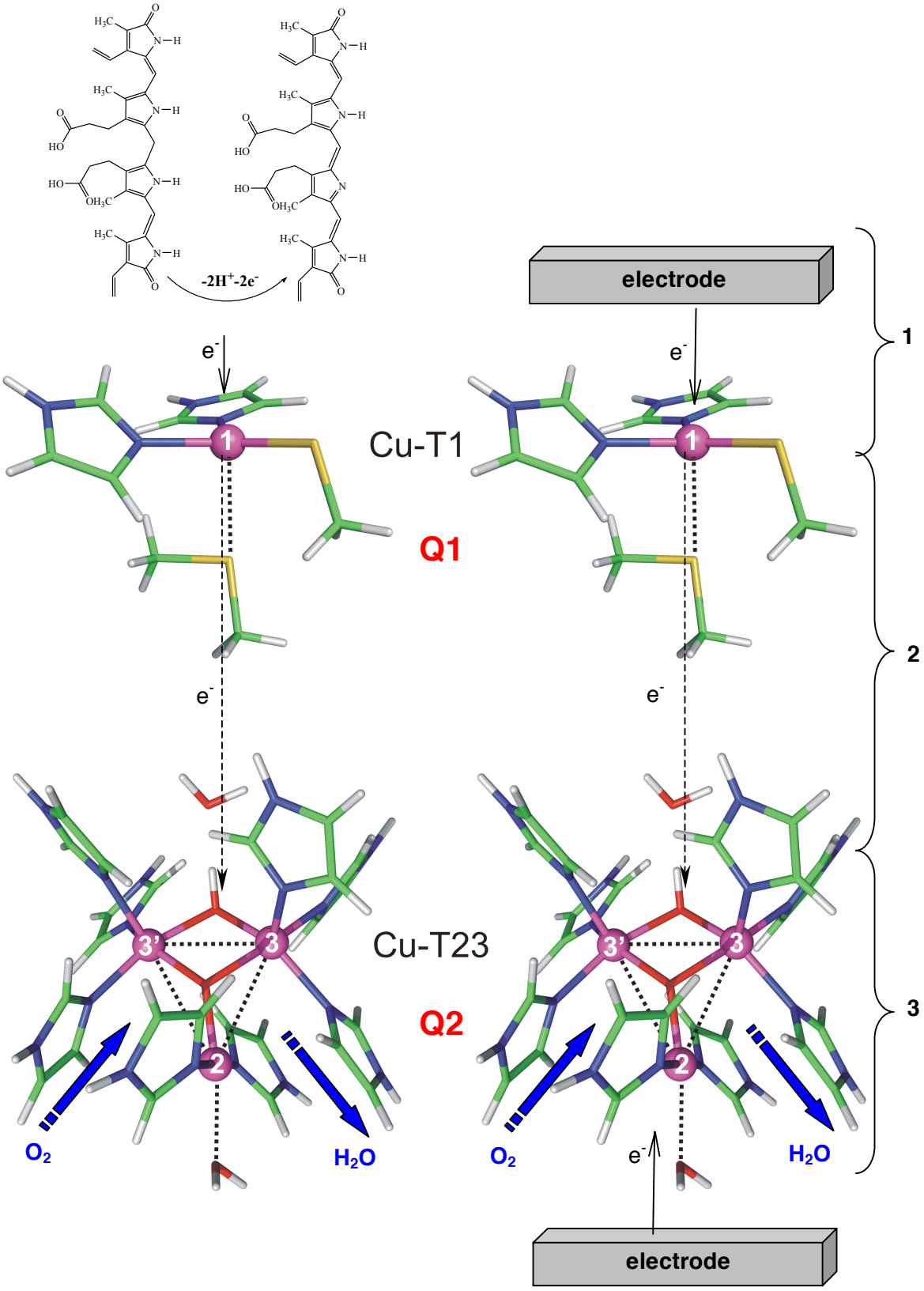

Figure 2

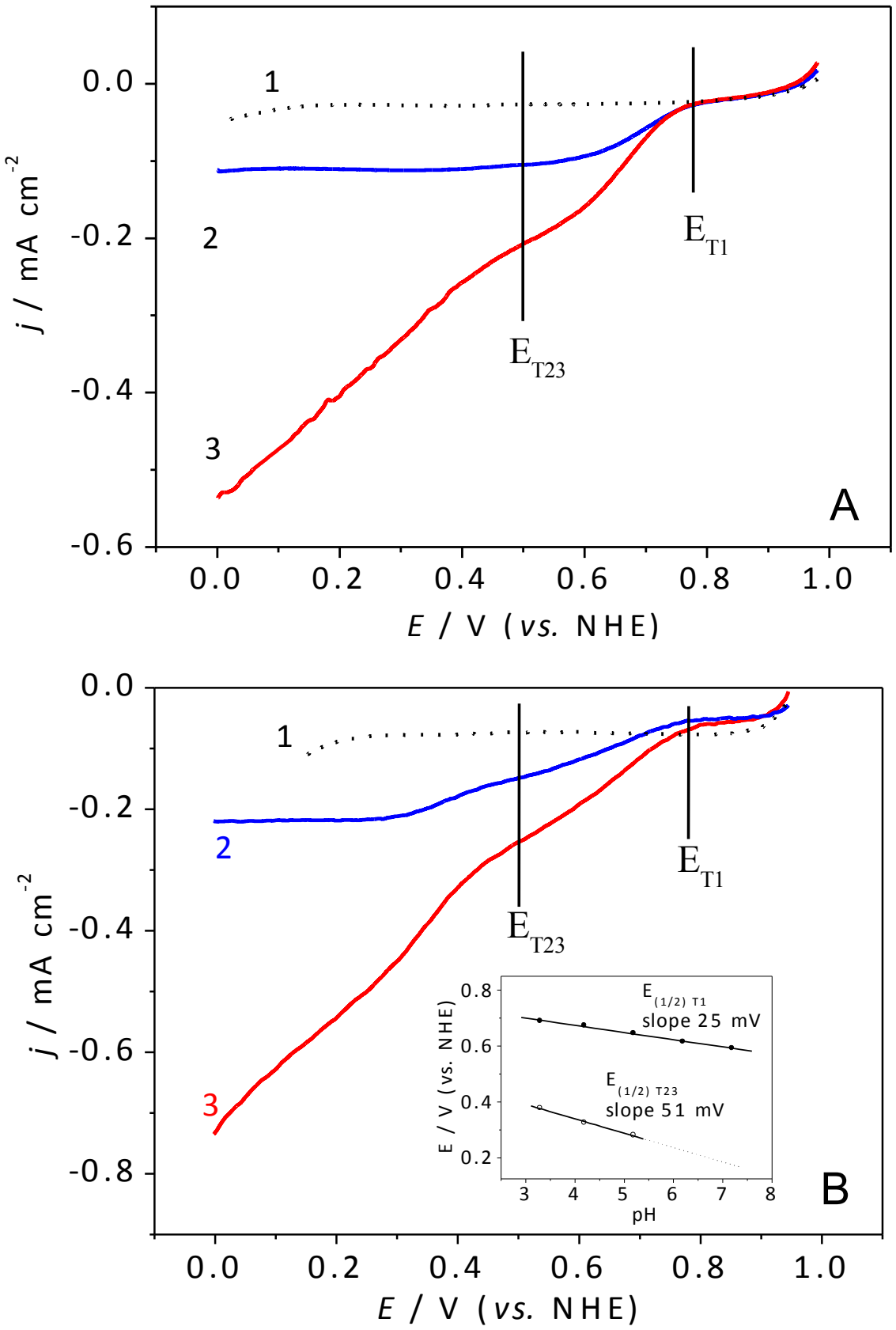
0.0
-0.2
-0.4
-0.6
j / mA cm-2
1
2
3
E T1
E T23
A
0.0
0.2
0.4
0.6
0.8
1.0
E / V (vs. NHE)
0.0
-0.2
-0.4
-0.6
-0.8
j / mA cm-2
1
2
3
E T1
E T23
E (1/2) T1
slope 25 mV
E (1/2) T23
slope 51 mV
E / V (vs. NHE)
0.8
0.6
0.4
0.2
3
4
5
6
7
8
pH
B
0.0
0.2
0.4
0.6
0.8
1.0
E / V (vs. NHE)

Figure 3

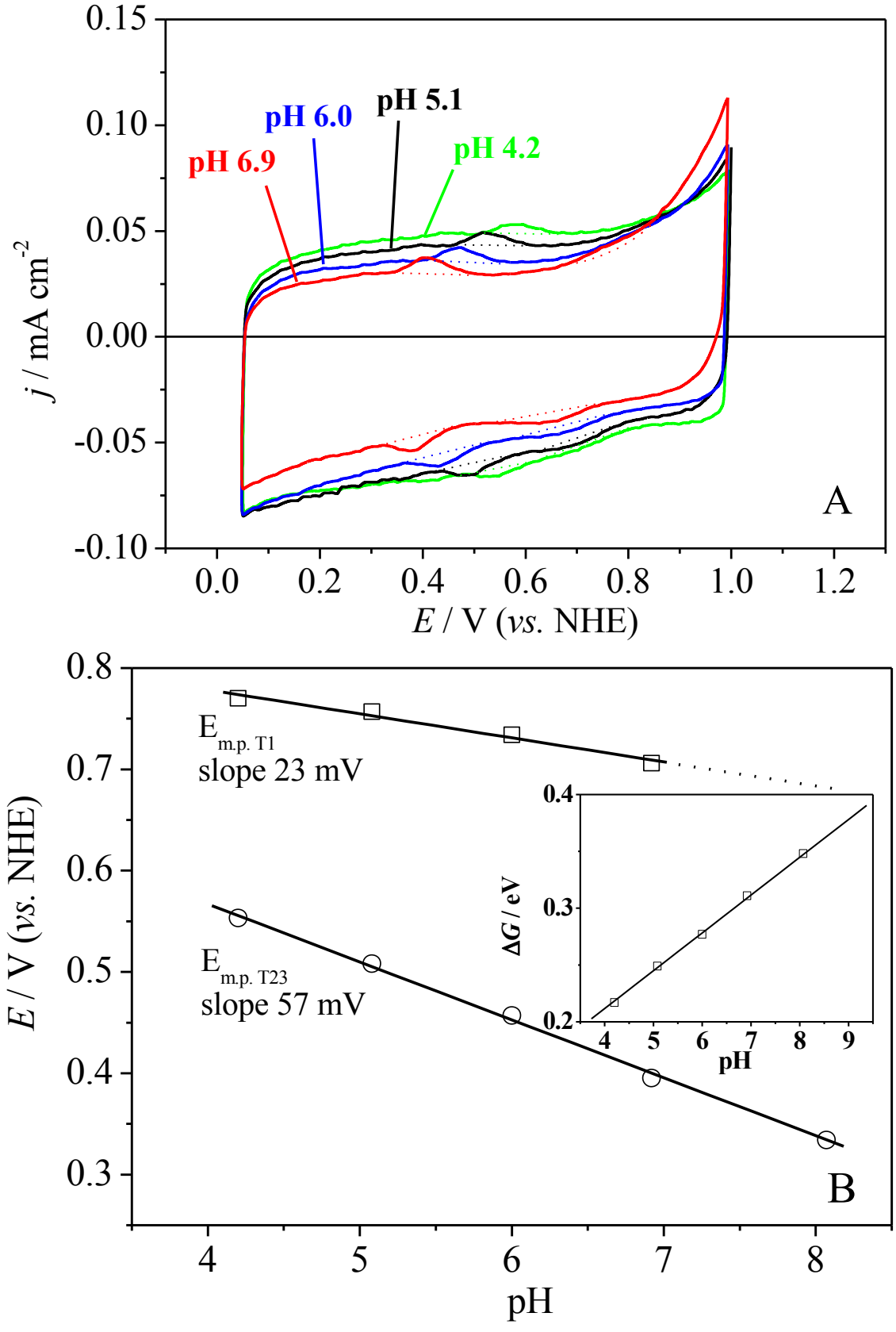
0.15
0.10
0.05
0.00
-0.05
-0.10
j / mA cm-2
pH 6.9
pH 6.0
pH 5.1
pH 4.2
A
0.0
0.2
0.4
0.6
0.8
1.0
1.2
E / V (vs. NHE)
0.8
0.7
0.6
0.5
0.4
0.3
E / V (vs. NHE)
Em.p. T1
slope 23 mV
Em.p. T23
slope 57 mV
ΔG / eV
0.4
0.3
0.2
4
5
6
7
8
9
pH
B
4
5
6
7
8
pH

Figure 4

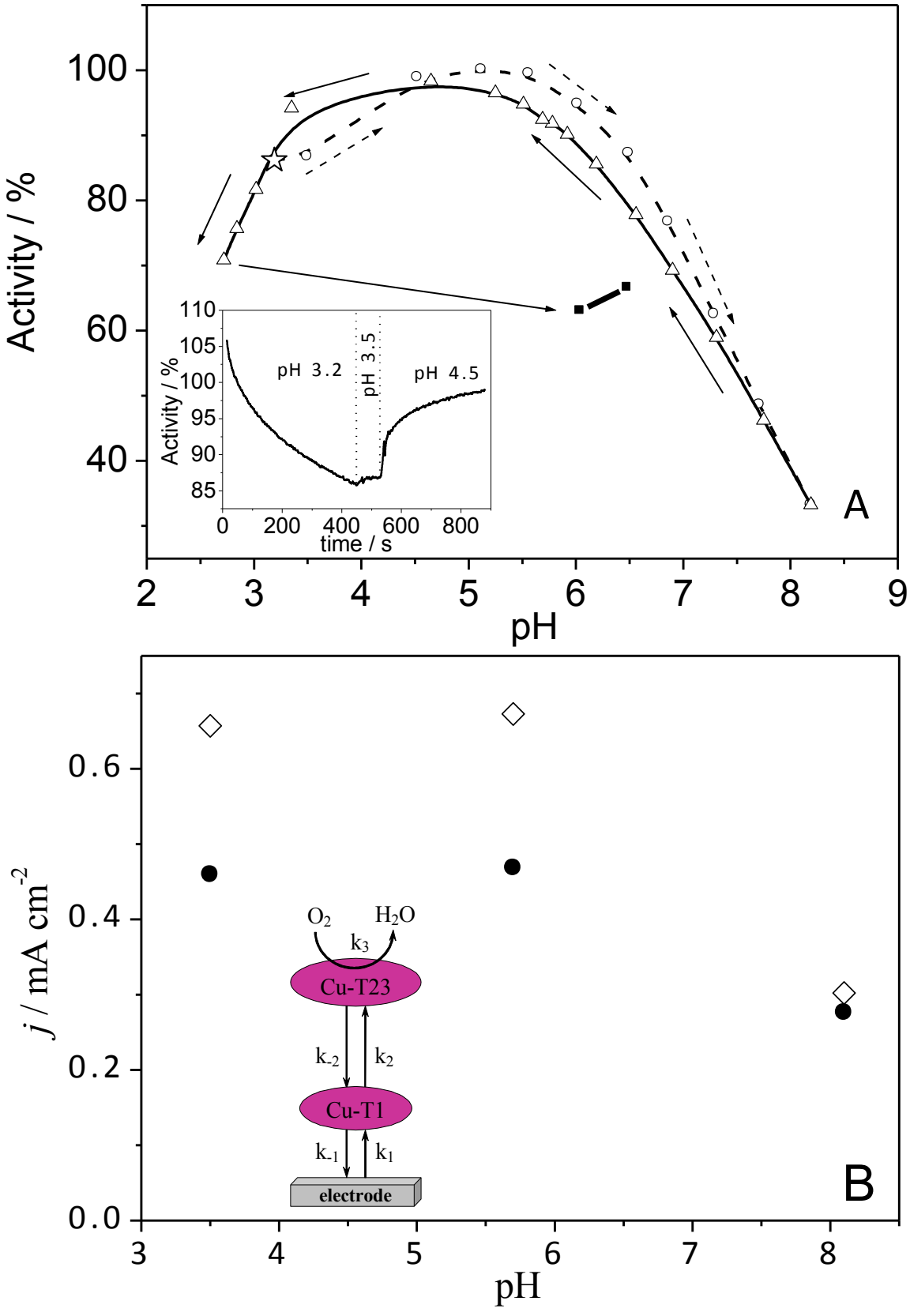
Activity / %
pH
A
Activity / %
time / s
pH 3.2
pH 3.5
pH 4.5
j / mA cm-2
B
O2
H2O
k3
Cu-T23
k-2
k2
Cu-T1
k-1
k1
electrode

Figure 5